

# **LiDAR Landslide Spatial Analysis at the Little Smoky River Highway 49 Crossing Site, Alberta (NTS 83N)**

**AER/AGS Open File Report 2013-14**

# **LiDAR Landslide Spatial Analysis at the Little Smoky River Highway 49 Crossing Site, Alberta (NTS 83N)**

A.J. Morgan, D.K. Chao, and C.R. Froese

Alberta Energy Regulator  
Alberta Geological Survey

January 2014

©Her Majesty the Queen in Right of Alberta, 2014  
ISBN 978-1-4601-0109-4

The Alberta Energy Regulator/Alberta Geological Survey (AER/AGS), its employees and contractors make no warranty, guarantee or representation, express or implied, or assume any legal liability regarding the correctness, accuracy, completeness or reliability of this publication. Any references to proprietary software and/or any use of proprietary data formats do not constitute endorsement by AER/AGS of any manufacturer's product.

If you use information from this publication in other publications or presentations, please acknowledge the AER/AGS. We recommend the following reference format:

Morgan, A.J., Chao, D.K. and Froese, C.R. (2014): LiDAR landslide spatial analysis at the Little Smoky River Highway 49 crossing site, Alberta (NTS 83N); Alberta Energy Regulator, AER/AGS Open File Report 2013-14, 30 p.

**Published January 2014 by:**

Alberta Energy Regulator  
Alberta Geological Survey  
4th Floor, Twin Atria Building  
4999 – 98th Avenue  
Edmonton, AB T6B 2X3  
Canada

Tel: 780.422.1927  
Fax: 780.422.1918  
E-mail: [AGS-Info@aer.ca](mailto:AGS-Info@aer.ca)  
Website: [www.ags.gov.ab.ca](http://www.ags.gov.ab.ca)

## Contents

Acknowledgements.....	vi
Abstract.....	vii
1 Introduction.....	1
1.1 Geological Setting.....	1
2 Landslide Classification.....	2
3 Instrumentation.....	3
3.1 Slope inclinometers.....	3
3.2 InSAR corner reflectors.....	3
3.3 Displacement results.....	6
4 Spatial Analyses.....	6
4.1 Slope Angle.....	6
4.2 Multiscale Spatial Analysis.....	9
4.2.1 Grid Creation and Statistics.....	11
4.2.2 Landslide Ranking Methodology.....	12
4.2.3 Landslide Ranking Results.....	15
5 Discussion and Conclusion.....	19
6 References.....	20
Appendix 1 – Landslide Key Map and Elevation Profiles.....	21
Appendix 2 – Grid Statistics.....	27

## Tables

Table 1. Minimum and maximum values obtained from the combined $SD_{\text{slope}}$ grid.....	11
Table 2. Mean, standard deviation, maximum, and minimum values calculated from the combined normalized $SD_{\text{slope}}$ grid.....	12
Table 3. Mean values calculated for each landslide area using the clipped normalized $SD_{\text{slope}}$ grid.....	13
Table 4. $SD_{\text{slope}}$ ranking scores for each landslide.....	15
Table 5. $SD_{\text{profile}}$ ranking scores for each landslide.....	16
Table 6. $SD_{\text{elevation}}$ ranking scores for each landslide.....	16
Table 7. Relative landslide surface texture total ranking score.....	17
Table 8. Minimum and maximum values obtained from the combined $SD_{\text{profile}}$ grid.....	27
Table 9. Mean, standard deviation, maximum, and minimum values calculated from the combined normalized $SD_{\text{profile}}$ grid.....	27
Table 10. Mean values calculated for each landslide area using the clipped normalized $SD_{\text{profile}}$ grid.....	28
Table 11. Minimum and maximum values obtained from the combined $SD_{\text{elevation}}$ grid.....	29
Table 12. Mean, standard deviation, maximum, and minimum values calculated from the combined normalized $SD_{\text{elevation}}$ grid.....	29
Table 13. Mean values calculated for each landslide area using the clipped normalized $SD_{\text{elevation}}$ grid.....	30

## Figures

Figure 1. Site location: Highway 49 crosses the Little Smoky River at latitude 55.459°N, longitude 117.149°W.....	2
Figure 2. Landslide boundaries shown on the LiDAR DEM.....	4
Figure 3. Slope inclinometer locations shown with displacement information.....	5
Figure 4. InSAR corner reflector locations with displacement vectors.....	5
Figure 5. Landslide boundary map showing the horizontal displacement ranges recorded by the slope inclinometers and GPS corner reflector measurements.....	7
Figure 6. Slope angle derivative map showing the distribution of slope angles for each landslide.....	8

Figure 7. Results of the morphological landslide comparison using the various slope angle derivative maps as an additional metric, showing the expected average horizontal displacement for slides without movement data.....10

Figure 8. Mean and standard deviation values calculated from the combined normalized  $SD_{\text{slope}}$  grid, which considers all the surface area across all the defined landslide polygons. ....13

Figure 9. Mean values calculated for  $SD_{\text{slope}}$  for each landslide ID compared to the mean for the combined normalized  $SD_{\text{slope}}$  grid with 1/6th standard deviation thresholds shown. ....14

Figure 10. Landslide map showing relative levels of surface roughness.

Figure 11. Key map showing landslide boundaries, identification numbers, and profile lines. ....21

Figure 12. Elevation profile lines for each landslide as shown in plan on Figure 11. ....26

Figure 13. Mean and standard deviation values calculated from the combined normalized  $SD_{\text{profile}}$  grid, which considers all the surface area across all the defined landslide polygons. ....27

Figure 14. Mean values calculated for  $SD_{\text{profile}}$  for each landslide ID compared to the mean for the combined normalized  $SD_{\text{profile}}$  grid, with 1/6th standard deviation thresholds shown. ....28

Figure 15. Mean and standard deviation values calculated from the combined normalized  $SD_{\text{elevation}}$  grid, which considers all the surface area across all the defined landslide polygons. 29

Figure 16.  $SD_{\text{elevation}}$  mean values calculated for  $SD_{\text{elevation}}$  for each landslide ID compared to the mean for the combined normalized  $SD_{\text{elevation}}$  grid, with 1/6th standard deviation thresholds shown. 30

## **Acknowledgements**

We thank R. Skirrow at Alberta Infrastructure and Transportation for providing the instrumentation data and valuable insight for this study and D. Medinski (former Alberta Geological Survey summer student) for summarizing the instrumentation results. T. Shipman (Alberta Geological Survey) critically read the draft of this report, and the authors thank him for his comments and suggestions.

## Abstract

Landslides within river valleys are relatively common in Alberta, notably so along rivers that have incised into glacial sediments and Cretaceous bedrock. A morphological approach using light detection and ranging (LiDAR), colour imagery, and displacement data was used to create an inventory of landslide features at the Little Smoky River Highway 49 crossing site. Spatial GIS analysis was performed using LiDAR data and commercially available software. Results were compared with the available displacement information in an attempt to relate surface texture attributes to landslide activity for known geological conditions. This method was assessed for its potential to generate an understanding of landslide types, processes, and relative levels of activity at sites that do not have displacement information but have similar geological conditions.

A bare-earth LiDAR digital elevation model was used to rank the landslides identified at the project site according to their surface roughness properties. Methodologies were derived from a study by Grohmann (2010) on multiscale analysis of topographic surfaces using standard deviation of slope ( $SD_{\text{slope}}$ ), profile curvature ( $SD_{\text{profile}}$ ), and elevation ( $SD_{\text{elevation}}$ ). Roughness calculations were performed using multiple window sizes on an area encompassing all of the identified landslides to generate a number of normalized grids from which mean and standard deviations values were calculated. The boundary of each landslide was used to clip these grids, and the mean surface roughness value was calculated for each landslide area. By applying user-defined thresholds based on standard deviation, each landslide was assigned a score based on the comparison of its mean roughness to the mean roughness of the combined landslide area, creating a relative roughness ranking for each landslide at the project site.

Preliminary results were comparable to field observations for the majority of landslides. However, the method tended to overestimate activity on the west side of the river crossing. This was likely a result of the unique morphology with large steep backscarps. The results presented in this report demonstrate that spatial analysis methods can provide useful metrics for the assessment of the relative activity state of landslides, but also highlight that a good understanding of the subsurface geological setting and expert judgement must be an integral part of the spatial analysis process.

# 1 Introduction

The bridge crossing of Highway 49 over the Little Smoky River is located in northwestern Alberta, approximately 45 km north of the Town of Valleyview (Figure 1). Deep-seated, slow-moving landslides located on the east and west valley slopes have affected the highway and bridge since bridge completion in 1958. Post-construction, it became apparent that the unstable valley slopes were affecting the west bridge abutment as well as the east and west bridge approaches (Skirrow et al., 2005). Ongoing mitigative measures, including changes to the bridge substructure and repairs to the roadway, have been successfully implemented over the years to allow the crossing infrastructure to remain functional despite the relatively slow but persistent slope movement.

Geotechnical monitoring techniques applied at the crossing site over the years have revealed the characteristics and rates of movement at the bridge crossing site. A series of slope inclinometers installed on both the east and west slopes have identified the depth and movement rate of failure planes. In addition, a differential interferometric synthetic aperture radar (InSAR) survey was carried out in 2003 in an attempt to understand the movement characteristics across the project site (Froese, 2004). More recently, a second InSAR survey was carried out using eighteen corner reflectors positioned at select locations around the bridge and road alignment (Froese et al., 2008).

This open file report summarizes the methods used to examine landslides at the project site and discusses the spatial analysis techniques used to investigate the activity of the unstable slopes. A high-resolution light detection and ranging (LiDAR) digital elevation model (DEM) was used in conjunction with aerial photos to assign discrete landslide boundaries based on the morphology at the crossing site, and instrumentation data was incorporated to determine the average rate of movement. Surface morphology properties for each landslide, obtained using spatial analysis, were examined for possible comparisons to areas without movement information to better understand the distribution of landslide activity within the river valley.

## 1.1 Geological Setting

The crossing of Highway 49 over the Little Smoky River has been the focus of a number of geotechnical and geological studies over the years. Thompson and Haley (1975) reported on the kinematics of slope instability at the project site and provided details of index properties of some of the different geological deposits. A comprehensive description of the physiography and geology at the Little Smoky and Highway 49 crossing has been written by Skirrow et al. (2005) as part of Alberta Transportation's ongoing project work at the bridge site. A summary of these more detailed explanations is provided below to familiarize the reader with the site.

The Little Smoky River is a tributary of the Peace River and has gently sloping, undulating valley walls with a relief of approximately 120 m from the prairie uplands to the river below. At the bridge crossing site, the Little Smoky River valley occupies a broad preglacial valley eroded into interbedded marine shales and sandstones of the Cretaceous-aged Smoky Group (Mollard and Associates, 1997). The preglacial valley was filled with till, inter-till sand, and glaciolacustrine deposits during glaciation. The glacial deposits that infill the preglacial valley have been eroded by river action following deglaciation. The valley walls have been formed from river downcutting and undermining of the slopes, creating deep-seated instabilities. This process is responsible for oversteepening the valley walls and causing large-scale, deep-seated landsliding that make up the irregular and relatively flat slopes of the present valley. Slope movements typically occur along the bedrock contact or within glaciolacustrine clay deposits that overlie bedrock.

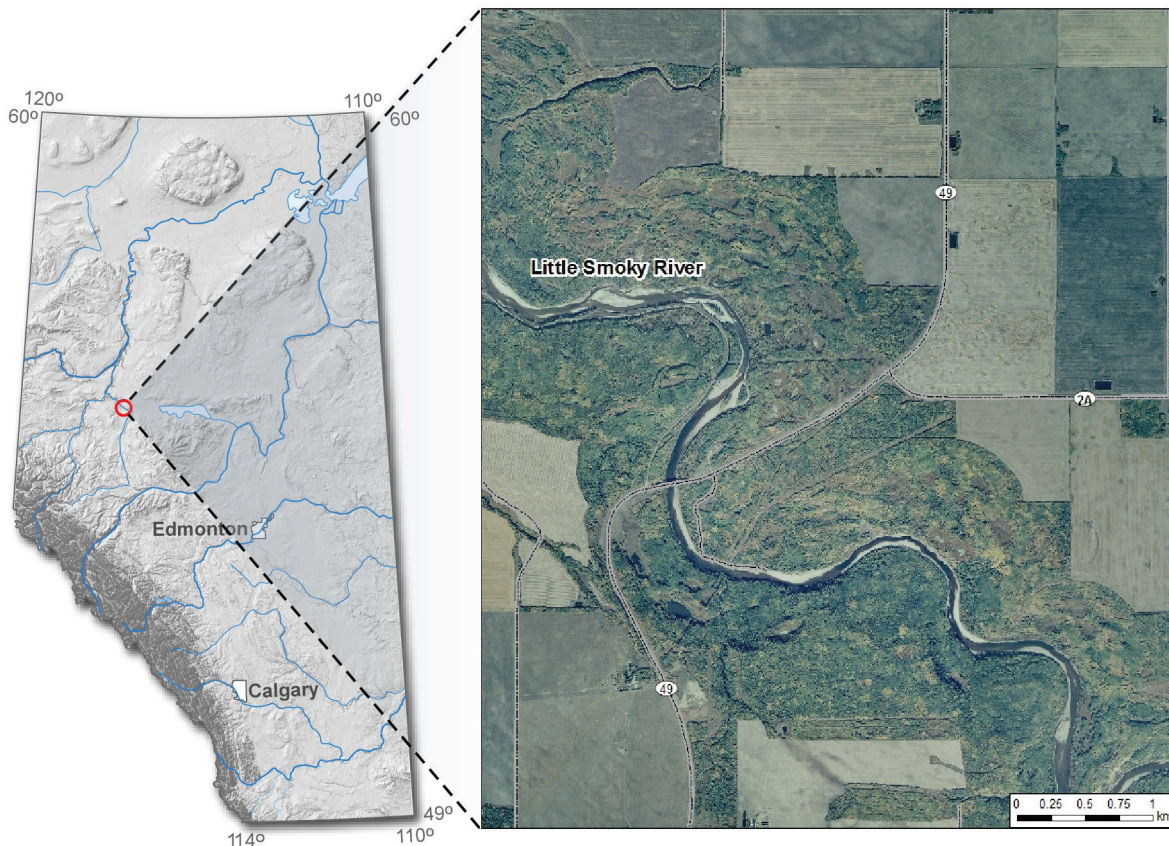


**Figure 1. Site location: Highway 49 crosses the Little Smoky River at latitude 55.459°N, longitude 117.149°W.**

## 2 Landslide Classification

LiDAR data with a 1 m horizontal resolution were utilized for the study area. The LiDAR data were processed to produce a bare-earth derivative, free of vegetation and man-made structures, which was then used as the DEM for landslide study purposes. Detailed morphological analysis of this DEM was undertaken to visually select boundaries for landslides that occur on the river valley slopes at the crossing site.

Application of a range of sun angles and azimuths were applied to this LiDAR DEM using GIS software. ArcGIS® produced shaded-relief images which highlight different aspects of the slide masses. The resulting series of shaded-relief images allowed the morphology of the river valley slopes to be examined at a very fine resolution. The next step was to develop boundaries for each landslide based on an idealized landslide morphology taken from Cruden and Varnes (1996). Field reconnaissance at the site assisted the creation of landslide boundaries in ArcGIS. In addition, colour airphoto imagery was helpful for differentiating the different slide events by examining vegetation distribution and scarp disturbance. A shaded-relief image of the LiDAR DEM with landslide boundaries generated in ArcGIS is shown in Figure 2.

Using the naming convention developed by Cruden and Varnes (1996), each landslide was assigned attributes based on the suggested type of movement. At the crossing site, the landslides are considered to be translational earth slides.

The landslides were also described based on activity, which has three components: state, distribution, and style. The crossing site failures are generally characterized as active, retrogressive, and complex and multiple landslides respectively.

Appendix 1 contains a key map (a figure showing the landslide identification numbers) as well as profile lines and corresponding profiles for each landslide (Figure 11 and Figure 12).

### **3 Instrumentation**

#### **3.1 Slope inclinometers**

Instrumentation at the project site began in the late 1960s with the installation of the first slope inclinometers in Alberta, which helped characterize landslide movements. Since that time, a number of exploratory boreholes and slope inclinometers have been installed; these inclinometers typically last three years before slope movement renders the instruments inoperable (Skirrow et al., 2005).

For this study, data from slope inclinometers installed and functional sometime between 2001 and 2008 were reviewed. Instruments that were installed to a depth extending beyond the deep-seated sliding surface were chosen, as they indicate important information as to the mechanism of sliding. The movement data indicate two adjoining slide zones on the west side of the river, one on each side of the bridge. The failure surface occurs in the marine shale between a depth of 35 m and an elevation of approximately 485 m.

The east side of the valley has a number of deep-seated failures of varying size and age. The instrumentation indicates that the failure surface occurs at an elevation of approximately 565 to 485 m, or approximately 55 m deep. Slope inclinometers on the east slope have been concentrated at a large embankment failure just north of the approach road and along the south flank of a large landslide. Figure 3 shows the distribution of slope inclinometers at the crossing site and indicates the recorded movement.

#### **3.2 InSAR corner reflectors**

In 2006, an array of 18 trihedral corner reflectors (CRs) was installed across the east and west slopes as part of a study which tested the applicability of corner reflector InSAR (CR-InSAR) for detecting slope movements in heavily vegetated terrain. These CR-InSAR measurements are only able to detect movement along the line of sight of the InSAR satellite. It is understood that this limitation means that movement in other directions is not detected. As a control for the satellite-based InSAR measurements, differential GPS measurements were made at each of these CRs from 2006 to 2007. In some cases, the horizontal component of the GPS measurement was found to be up to 4 times greater than the horizontal displacement measured by the CR-InSAR. For the purposes of this study, only the horizontal component of the GPS measurements were considered, as they better reflect the surface displacement characteristics of the landslides. Further information regarding a discussion of the CR-InSAR results can be found in Froese et al. (2008). Figure 4 shows the location of the CRs and indicates the movement magnitude and direction as measured by the differential GPS system.



Figure 2. Landslide boundaries shown on the LiDAR DEM.

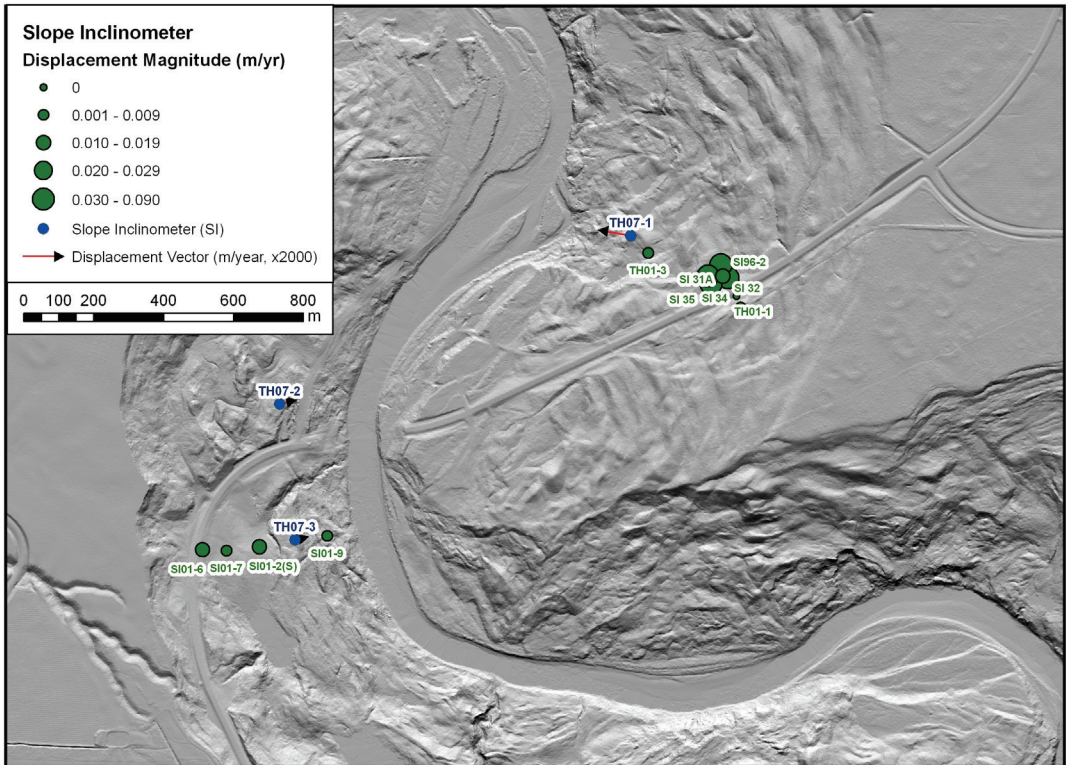


Figure 3. Slope inclinometer locations shown with displacement information. Note that the displacement vector magnitude is exaggerated 2000 times for display purposes.

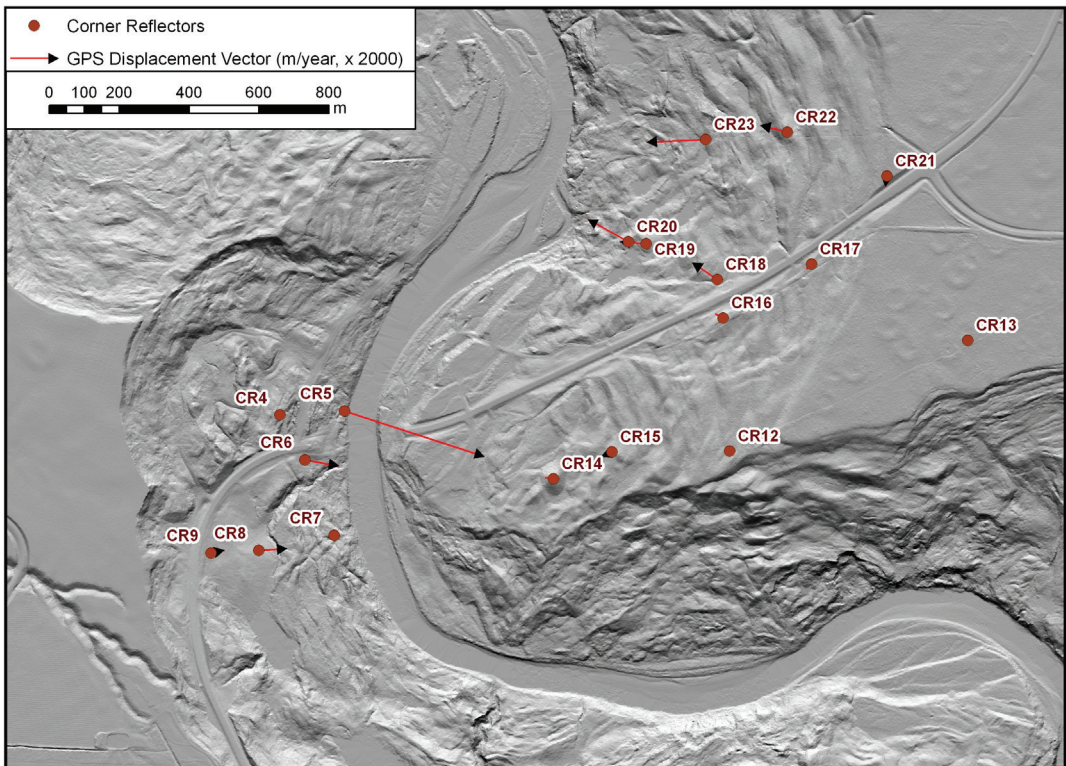


Figure 4. InSAR corner reflector locations with displacement vectors. Note that displacement magnitude is exaggerated 2000 times for display purposes.

### 3.3 Displacement results

Slope inclinometer measurements on the east valley slope indicate average horizontal movement rates from 8 to 24 mm/year from 2001 to 2008. In comparison, the CR GPS measurements on the east valley slope indicate an average surface horizontal displacement ranging from 8 to 49 mm/year for the majority of the CR installations, and a relatively high reading of 210 mm/year recorded at CR5. It should be noted that CR5 is located on the outside bend of the river course where the highest rate of river erosion is expected.

Data from the western slope inclinometers indicate average horizontal movement rates in the order of 7 to 86 mm/year as measured from 2001 to 2008. The CRs on the west slope indicate a similar range of average horizontal displacement of 6 to 85 mm/year as recorded by the GPS system. As Figure 3 and Figure 4 show, the CR installations provide better spatial coverage of the western slope landslides than the slope inclinometer installations.

These horizontal displacement data were combined with the landslide inventory discussed in Section 2 to produce a landslide activity map displaying the various ranges of horizontal movement for each landslide. Note that only 8 of the 14 landslides identified at the site have displacement information measured by slope inclinometers and CR GPS measurements. Figure 5 shows the measured horizontal displacement ranges for each landslide.

Based on the measured movement rates at the crossing site, it is clear that the east and west slopes are moving rather slowly. Using the Cruden and Varnes (1996) velocity scale, the instrumented landslides are classified as very slow ( $>16$  mm/year and  $< 1.6$  m/year) and extremely slow ( $< 16$  mm/year).

## 4 Spatial Analyses

### 4.1 Slope Angle

The distribution of slope angle was considered as an aid to empirically estimating the activity of those landslides at the project site for which there were no measured displacement data.

The SLOPE function was used in ArcGIS to first look at the average slope angle across each landslide polygon. Profiles of each landslide are shown in Appendix 1 along with a key map indicating the landslide ID and the profile line as measured. The east valley slope landslides have average slope angles ranging from approximately 9 to 16 degrees, and the west valley slope landslides range from 13 to 16 degrees. It was observed that the larger and deeper-seated landslides located on the eastern valley slope generally showed larger yearly horizontal displacements at lower average slope angles than the west slope. This could be a result of the deeper failure surface on the east slope (~55 m) versus the east slope (~35 m).

A slope angle map was derived from the LiDAR DEM data to show the distribution of slope angle within a landslide polygon. Figure 6 shows an example of such a derivative map, where the slope angle distribution has been displayed based on a slope angle of 14 degrees. The shading of the derivative map shows areas of the slope greater than 14 degrees and less than or equal to 14 degrees.

Slope angle derivative maps were prepared for angles ranging from 9 to 16 degrees. The area for each landslide polygon was then calculated, and the per cent area above the selected slope angle and the per cent area less than or equal to the selected slope angle were calculated and tabulated for each landslide polygon.

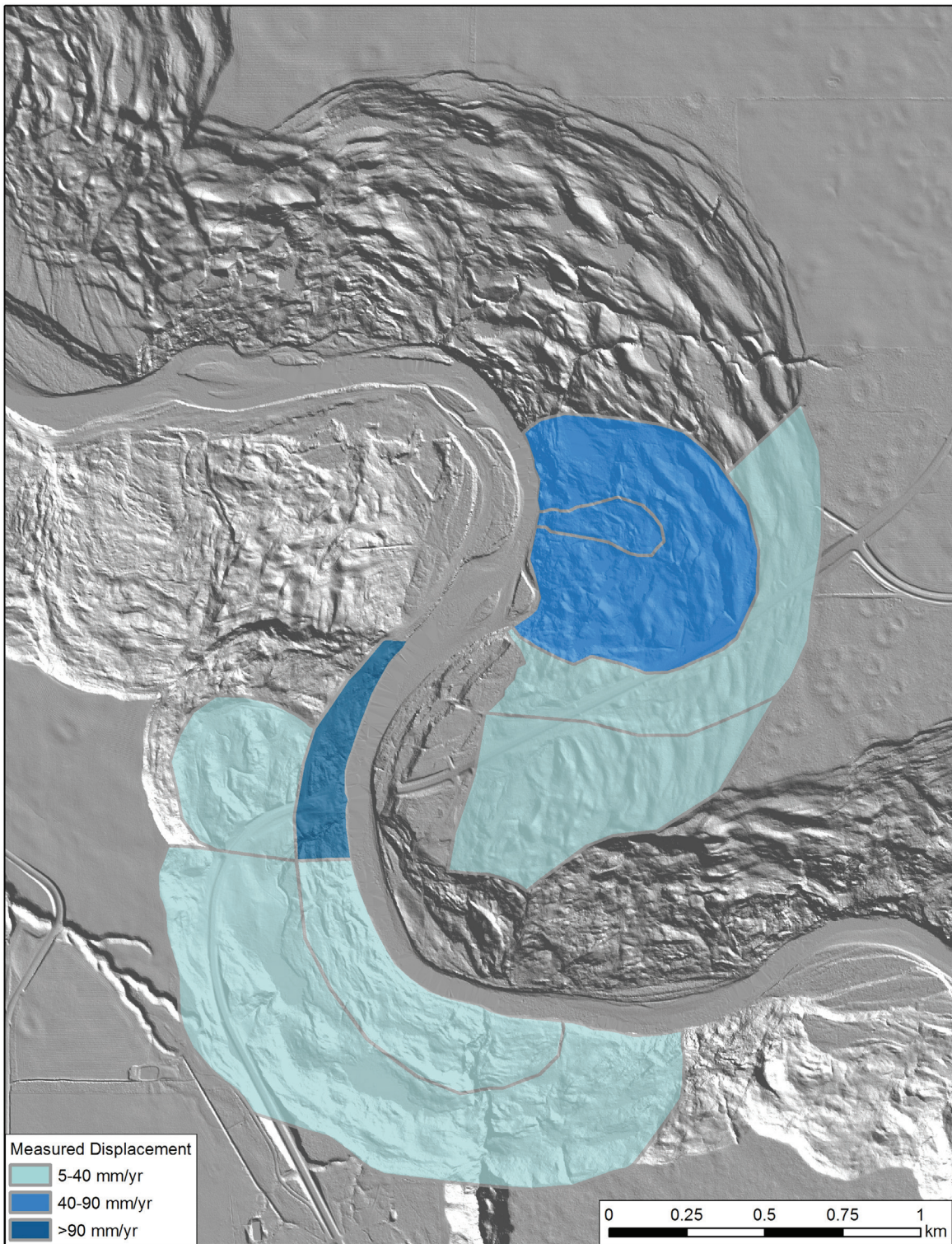


**Figure 5. Landslide boundary map showing the horizontal displacement ranges recorded by the slope inclinometers and GPS corner reflector measurements.**



Figure 6. Slope angle derivative map showing the distribution of slope angles for each landslide.

The breakdown of slope angle by per cent area was then examined to see if there was any relationship between movement rate of the landslides and the division of slope angle by per cent area. The intent was to find a way to relate the morphological signature of a landslide with a known movement to slides without movement data, thereby empirically estimating the expected movement.

As a control, landslides without movement data were also compared to those with movement data using a traditional visual morphological comparison of the surface texture of the DEM, airphoto imagery, and the slope angle derivative maps. This comparison was used as the primary method for choosing the expected movement range for those landslides without movement data.

For consistency, landslides on the east valley slope with movement data were compared to those eastern landslides without movement data. The same was done for the western slope landslides. As mentioned earlier in this section, the eastern slides tend to be larger and deeper seated than the western slides and, in some cases, have greater average yearly horizontal displacements at lower slope angles than the western slides.

The comparison of slope angle division by per cent area was not always conclusive. In a few instances, the per cent area comparison did match the result of the morphological visual comparison, yielding a similar expected displacement range for slides without movement data. However, it was found that relying on slope angle per cent area alone could provide a misleading result for expected displacement.

It was found that comparing slope angle per cent area as described has limited usefulness in determining a specific morphological signature that is directly related to landslide activity. This is primarily due to the fact that the per cent area comparison is an absolute one—that is, it does not account for the differences in slope angle distribution between slides. This approach might imply that a landslide having a few large failure scarps above a chosen angle has similar displacement as a landslide with many small failure scarps above the same angle, so long as the per cent areas are similar. However, the slope angle derivative map is considered a useful addition to the traditional approach to landslide characterization and classification in that it provides yet another means to visually consider and compare slope morphology. Figure 7 shows the result of the empirical-based landslide comparison and depicts the predicted average horizontal displacement rates for the un-instrumented landslides at the site.

## **4.2 Multiscale Spatial Analysis**

The spatial analysis used for the Little Smoky study area builds on earlier work on landslide classification outlined in Morgan and Chao (2013). Three spatial analyses are used. Each of the three analyses first determines surface texture for an area that encompasses all the landslides within the study area. The resulting data are then normalized. The surface texture of each individual landslide is then calculated using the normalized data. This allows for each landslide to be indexed based on its individual surface texture signature as compared to the signature across all landslides together, creating a relative scale of surface texture or roughness from least rough to most rough.

This analysis tests the assumption that a relationship exists between the activity of the landslide and its surface texture, as available movement data within the Little Smoky project site allows for a comparison of the calculated surface texture to the measured displacement. For those landslides that do not have movement data, an empirical estimation of landslide activity can be made by comparing their relative roughness ranking to the relative roughness ranking of landslides with movement data.

The functions used for determining surface texture or roughness are derived from a study by Grohmann et al. (2010) on multiscale analysis of a topographic surface from a DEM. They described six functions for analyzing surface roughness, and we have adopted three of these for our analysis. They are standard

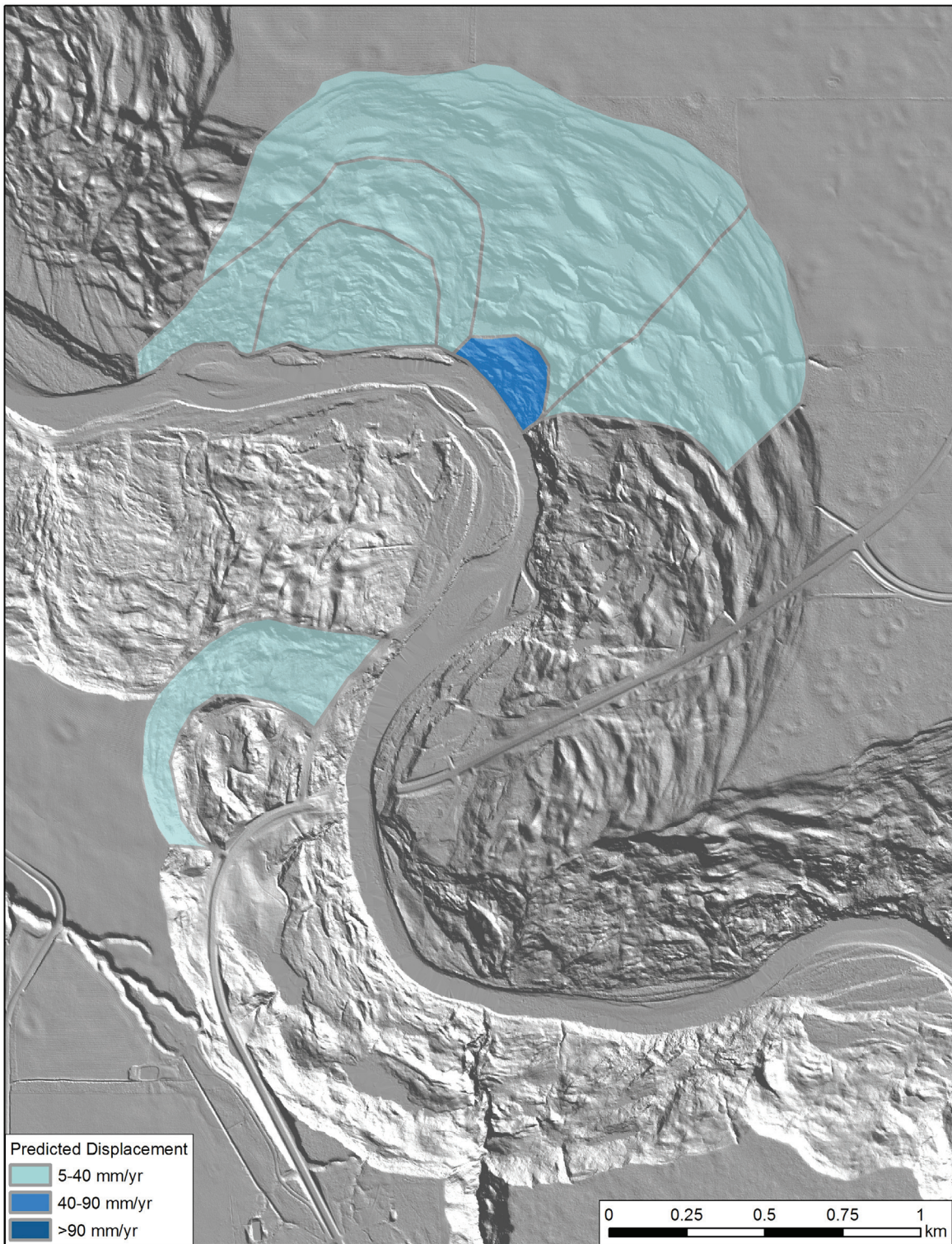


**Figure 7. Results of the morphological landslide comparison using the various slope angle derivative maps as an additional metric, showing the expected average horizontal displacement for slides without movement data.**

deviation of slope ( $SD_{\text{slope}}$ ), profile curvature ( $SD_{\text{profile}}$ ), and elevation ( $SD_{\text{elevation}}$ ). These techniques were chosen because they did not require any data manipulation such as detrending; they were easily applied using readily available software and were well suited to our high resolution LiDAR DEM as input data.

Each analytical technique has its advantages and limitations.  $SD_{\text{slope}}$  can identify steep slopes, areas of surface cluster, and breaks of slope.  $SD_{\text{elevation}}$  can detect breaks of slope and regional relief. Both  $SD_{\text{slope}}$  and  $SD_{\text{elevation}}$  perform well at any scale; however, they might enhance noise or error in a DEM.  $SD_{\text{profile}}$  can identify breaks of slope but not as well as  $SD_{\text{slope}}$ , and it is sensitive to DEM noise. These shortfalls are somewhat compensated by the vertical and horizontal accuracy of the LiDAR data at 0.35 m and 0.45 m, respectively, and reduction of noise in the processed bare-earth DEM from resampling the resolution of the LiDAR data from from 1 m to 3 m. In addition, a multiscale approach was used for the spatial analysis with five moving window sizes— $3\times 3$ ,  $5\times 5$ ,  $7\times 7$ ,  $9\times 9$ , and  $11\times 11$ —which minimizes the effect of localized topological bias.

#### 4.2.1 Grid Creation and Statistics

Grids and statistics are generated from the LiDAR DEM using existing functions available in ArcGIS. Results are exported to Microsoft Excel for the determination of landslide ranking discussed in Section 4.2.2. An explanation is provided below for the creation of surface texture grids and corresponding statistics for the SLOPE function with the understanding that the other two methods follow the same workflow:

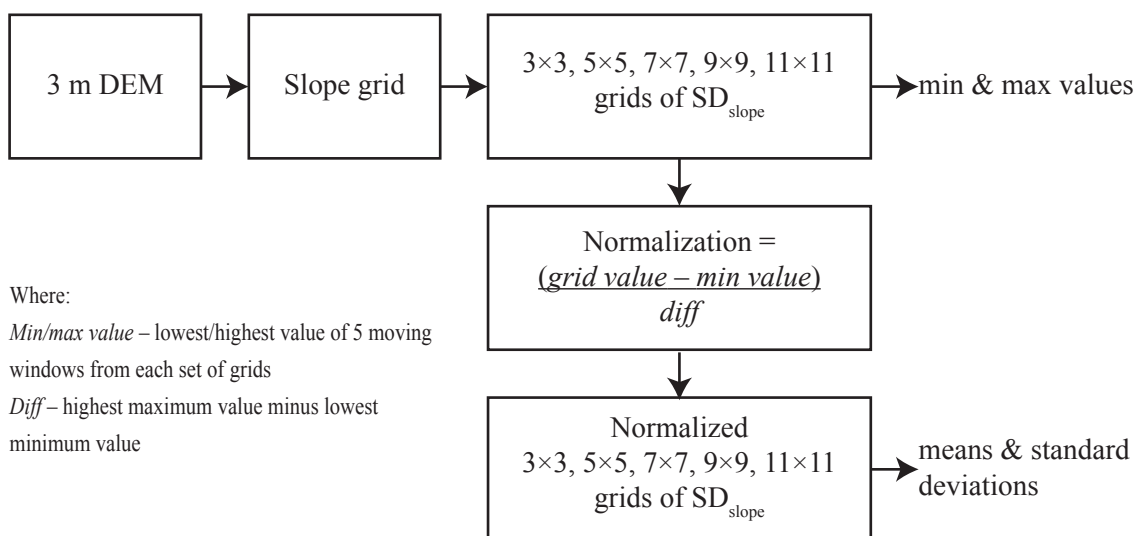
- 1) Grids are derived from the 3 m DEM in ArcGIS using the SLOPE function for all of the landslides combined into one area.
- 2) This grid becomes the input for the focal statistical function in ArcGIS Spatial Analyst with ‘Standard Deviation’ selected as the option to generate a  $SD_{\text{slope}}$  grid for each of the five moving window sizes:  $3\times 3$ ,  $5\times 5$ ,  $7\times 7$ ,  $9\times 9$  and  $11\times 11$ .
- 3) The minimum and maximum values are captured for each moving window size (Table 1).
- 4) To create a better understanding of the overall change of slope between the different landslides across the study area, and to minimize scale bias, we normalize the grid for each moving window size to contain values between 0 and 1, using the absolute minimum and maximum values calculated across all five moving window sizes. These grids are referred to as the combined normalized SD grids.
- 5) Mean and standard deviation values are calculated for each moving window size from the corresponding combined normalized SD grid.
- 6) Mean values are calculated for the area within each landslide boundary by using the landslide polygon shapefile to clip the corresponding area from the combined normalized SD grid for each moving window size.

**Table 1. Minimum and maximum values obtained from the combined  $SD_{\text{slope}}$  grid. These values are used to normalize the grid and create the combined normalized  $SD_{\text{slope}}$  grid.**

$SD_{\text{slope}}$	$3\times 3$	$5\times 5$	$7\times 7$	$9\times 9$	$11\times 11$
Min	0.00293012	0.03347457	0.04109905	0.07818767	0.10776677
Max	23.3437519	22.9027081	22.7279568	22.4625912	20.4803658

Diff = 23.3408218

The graphic below summarizes the grid and statistic generation workflow:



#### 4.2.2 Landslide Ranking Methodology

In order to rank each landslide according to its surface texture or roughness, the surface texture within each landslide boundary is compared to the surface texture across all the landslides combined, effectively providing a relative scale of surface texture, or roughness, across the site. Mean and standard deviation values are first calculated for the combined normalized SD grid using ArcGIS Spatial Analyst. Results are shown in Figure 8 and Table 2.

A GIS shapefile with landslide boundaries (Figure 2) is used to clip the combined normalized SD grid for each landslide polygon. The mean value within the area defined by each landslide polygon is then calculated. Table 3 and Figure 9 detail the mean values generated for each landslide. The landslides are ranked according to how their mean surface texture value compares to the mean value of the combined grid, which considers the surface texture across all the landslides combined. A user-defined threshold of standard deviation generated from the combined normalized grid is used for the comparison. For this study, a user-defined standard deviation of 1/6th was used and is shown in Figure 8 and Figure 9.

**Table 2. Mean, standard deviation, maximum, and minimum values calculated from the combined normalized  $SD_{\text{slope}}$  grid.**

	3x3	5x5	7x7	9x9	11x11
Mean	0.15487	0.19532	0.22130	0.24006	0.25448
Std Dev	0.09992	0.10999	0.11351	0.11434	0.11327
Max	0.17152	0.21365	0.24022	0.25912	0.27336
Min	0.13822	0.17699	0.20238	0.22100	0.23560

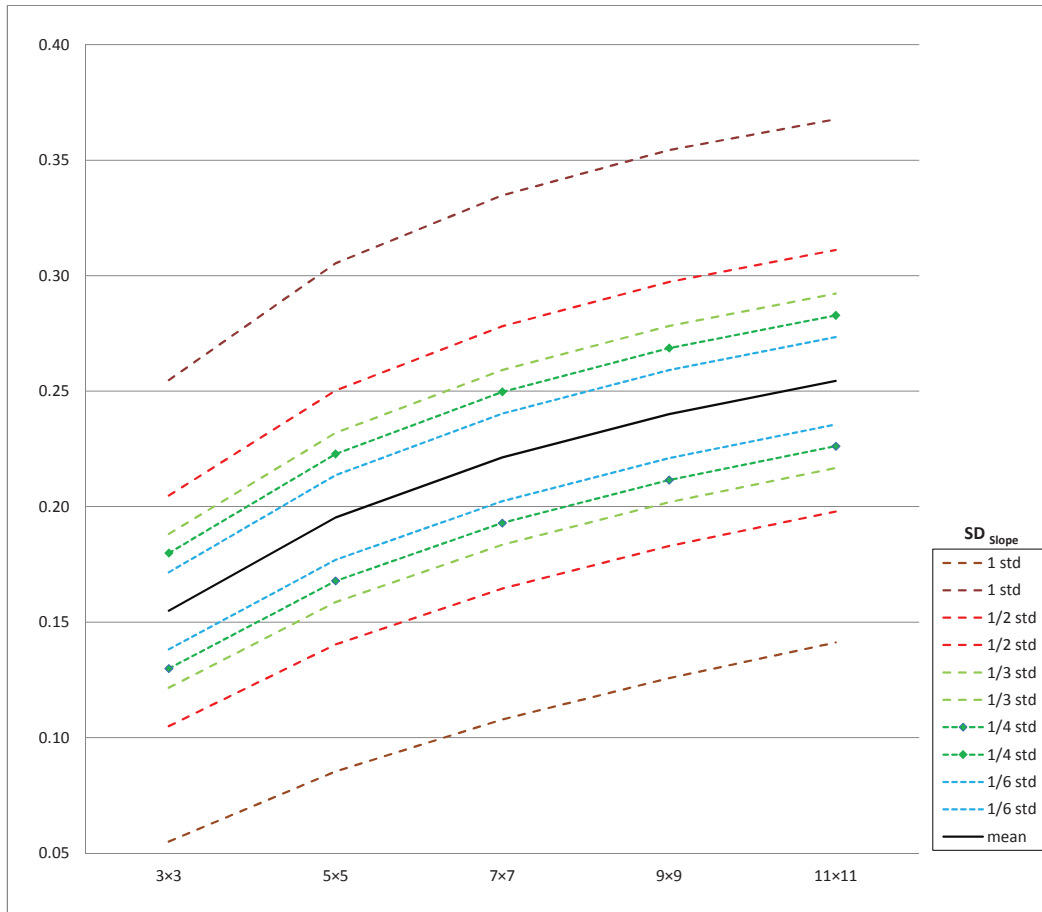
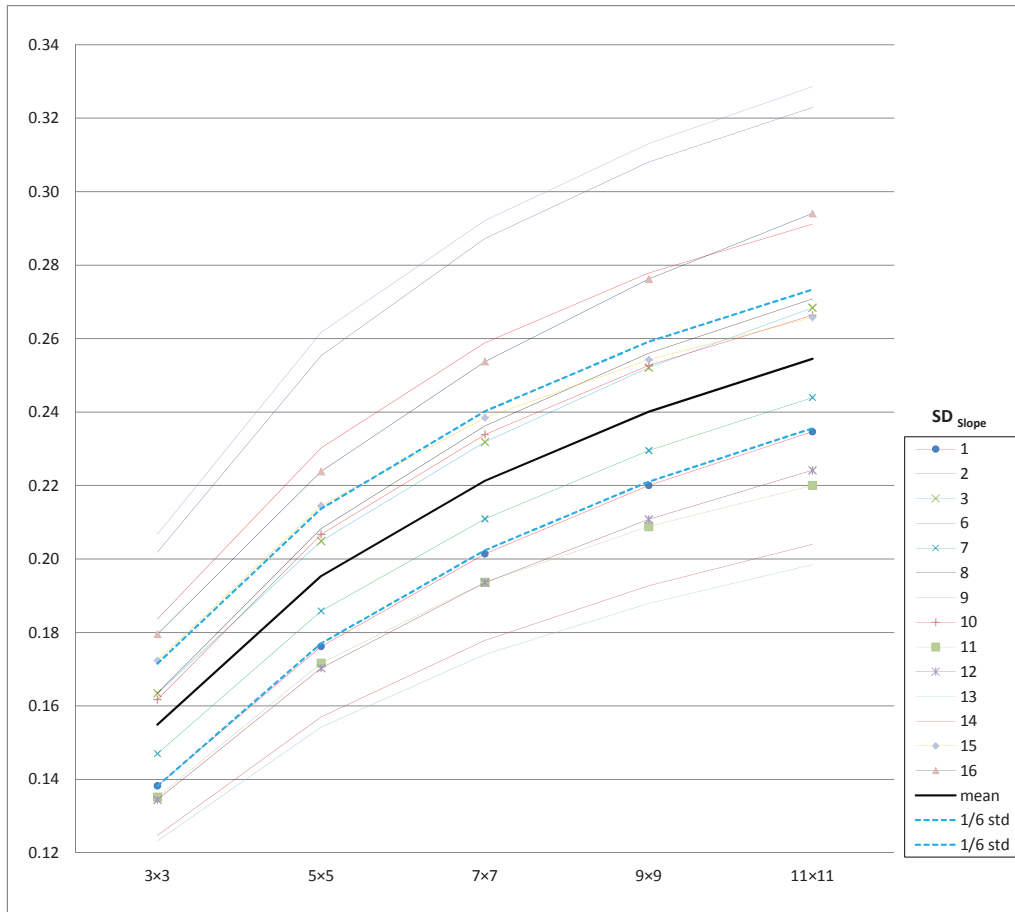


Figure 8. Mean and standard deviation values calculated from the combined normalized  $SD_{slope}$  grid, which considers all the surface area across all the defined landslide polygons.

Table 3. Mean values calculated for each landslide area using the clipped normalized  $SD_{slope}$  grid.

$SD_{slope}$ – Mean Values						
Landslide ID	3x3	5x5	7x7	9x9	11x11	
1	0.13822	0.17618	0.20137	0.22001	0.23465	
2	0.12475	0.15701	0.17782	0.19273	0.20402	
3	0.16342	0.20488	0.23184	0.25211	0.26840	
6	0.20185	0.25538	0.28723	0.30808	0.32293	
7	0.14702	0.18584	0.21094	0.22952	0.24395	
8	0.16352	0.20822	0.23625	0.25601	0.27084	
9	0.20673	0.26167	0.29213	0.31308	0.32860	
10	0.16174	0.20672	0.23392	0.25266	0.26636	
11	0.13515	0.17165	0.19364	0.20883	0.22001	
12	0.13444	0.17031	0.19359	0.21077	0.22415	
13	0.12323	0.15424	0.17401	0.18791	0.19845	
14	0.18369	0.23022	0.25890	0.27783	0.29114	
15	0.17237	0.21448	0.23847	0.25426	0.26580	
16	0.17952	0.22383	0.25371	0.27621	0.29407	



**Figure 9. Mean values calculated for  $SD_{slope}$  for each landslide ID (coloured lines) compared to the mean for the combined normalized  $SD_{slope}$  grid (black line) with 1/6th standard deviation thresholds shown (SD).**

A score of 1, 2, or 3 is assigned to a landslide if its mean value ranks lower, within, or higher, respectively, than the mean value for the entire combined normalized SD grid using the upper and lower limits of the user-defined threshold. Figure 9 plots the  $SD_{slope}$  mean values calculated for each landslide, the mean value for all the landslides combined, as well as the threshold value of 1/6th SD calculated from the combined SD grid across all the landslides.

Rankings are performed on all five moving window grids separately. They are each assigned a score and then summed to create a total score for each landslide. Threshold values are determined by adding and subtracting a fraction of the standard deviation from the mean value calculated for each landslide. For this study area, 1/6th of a standard deviation was chosen as it provided reasonable landslide ranking results based on the known slope displacements.

For example, the mean and standard deviation of the normalized 3x3 grid are 0.15487 and 0.09992 (Table 2). Its threshold values of

$$\text{Upper limit: } 0.15487 + (0.09992 \div 6) = 0.17152$$

$$\text{Lower limit: } 0.15487 - (0.09992 \div 6) = 0.12822$$

Individual landslides with mean values  $> 0.15487$  will get a score of 3, those with mean values  $\leq 0.15487$  and  $\geq 0.12822$  will be assigned a 2, and those with mean values  $< 0.12822$  get a score of 1. Scores of all five moving windows from each landslide are summed for a total score ranging from 5 to 15. They indicate the relative change of slope, where 5 is low and 15 is high. Table 4 lists the scoring results for  $SD_{\text{slope}}$ .

**Table 4.  $SD_{\text{slope}}$  ranking scores for each landslide.**

Landslide ID	$SD_{\text{slope}}$ – Ranking Scores					Total
	3×3	5×5	7×7	9×9	11×11	
1	2	1	1	1	1	6
2	1	1	1	1	1	5
3	2	2	2	2	2	10
6	3	3	3	3	3	15
7	2	2	2	2	2	10
8	2	2	2	2	2	10
9	3	3	3	3	3	15
10	2	2	2	2	2	10
11	1	1	1	1	1	5
12	1	1	1	1	1	5
13	1	1	1	1	1	5
14	3	3	3	3	3	15
15	3	3	2	2	2	12
16	3	3	3	3	3	15

The same procedure is followed to determine the relative surface texture score using the  $SD_{\text{profile}}$  and  $SD_{\text{elevation}}$  grids. For simplicity, only the ranking results are shown below for the  $SD_{\text{profile}}$  and  $SD_{\text{elevation}}$  grids. For further detail, the reader can refer to Appendix 2, which lists the calculated values used to normalize the combined SD grids, mean and standard deviation values for the combined normalized SD grids (profile and elevation), and the mean surface texture values.

### 4.2.3 Landslide Ranking Results

#### $SD_{\text{slope}}$

The scoring results for  $SD_{\text{slope}}$ , shown in Table 4, show that most landslides have a consistent score across all moving window sizes. The mean  $SD_{\text{slope}}$  values of slides 1, 2, 11, 12, and 13 are below the lower limit of the 1/6th SD threshold, indicating a lower variation in slope changes than the entire landslide system (Figure 9). Slides 3, 7, 8, and 10 fall within the 1/6th SD threshold, and therefore they have a similar level of variation as the overall landslide system. Slides 6, 9, 10, 14, 15, and 16 are above the upper limit of the 1/6th SD threshold, indicating a higher variation than the entire landslide system. Furthermore, both slide 1 and 15 show a decrease of  $SD_{\text{slope}}$  ranking scores (Table 4). The score for slide 1 drops from 2 to 1 after the 5×5 window while that for slide 15 drops from 3 to 2 after 7×7 window. These decreases reflect a general change of slope from high to low relief within those individual slides.

#### $SD_{\text{profile}}$

Analysis of  $SD_{\text{profile}}$  (Table 5) shows similar results to  $SD_{\text{slope}}$  rankings, in that most landslides have a consistent value across all moving window sizes. The mean  $SD_{\text{profile}}$  values of slides 1, 2, 11, 12, and 13

are below the lower limit of the 1/6th SD threshold and therefore have less variation in profile changes than the entire landslide system (Figure 14 in Appendix 2). Slides 7, 8, and 10 fall within 1/6th SD threshold and have a similar level of variation as the overall landslide system. Slides 3, 6, 9, 14, 15, and 16 are above upper limit of the 1/6th SD threshold, indicating a higher level of variation than the overall landslide system. The  $SD_{profile}$  ranking score of slide 3 (Table 5) shows an increase from 2 to 3 after the 7×7 window, and the score of slide 11 decreases from 2 to 1 after the 9×9 window. These changes show a general change of slope profile within those individual landslides.

**Table 5.  $SD_{profile}$  ranking scores for each landslide.**

Landslide ID	$SD_{profile}$ – Ranking Scores					Total
	3×3	5×5	7×7	9×9	11×11	
1	1	1	1	1	1	5
2	1	1	1	1	1	5
3	2	2	2	3	3	12
6	3	3	3	3	3	15
7	2	2	2	2	2	10
8	2	2	2	2	2	10
9	3	3	3	3	3	15
10	2	2	2	2	2	10
11	2	2	2	2	1	9
12	1	1	1	1	1	5
13	1	1	1	1	1	5
14	3	3	3	3	3	15
15	3	3	3	3	3	15
16	3	3	3	3	3	15

**$SD_{elevation}$**

Analysis of  $SD_{elevation}$  shows that all landslides have a consistent value across all moving window sizes (Table 6). The mean  $SD_{elevation}$  values of slides 1, 2, 11, 12, and 13 are below the lower limit of the 1/6th threshold while slides 3, 7, 8, 10, and 15 fall within the threshold, and slides 6, 9, 14, and 16 are above its upper limit (Figure 16 in Appendix 2).

**Table 6.  $SD_{elevation}$  ranking scores for each landslide.**

Landslide ID	$SD_{elevation}$ – Ranking Scores					Total
	3×3	5×5	7×7	9×9	11×11	
1	1	1	1	1	1	5
2	1	1	1	1	1	5
3	2	2	2	2	2	10
6	3	3	3	3	3	15
7	2	2	2	2	2	10
8	2	2	2	2	2	10
9	3	3	3	3	3	15
10	2	2	2	2	2	10
11	1	1	1	1	1	5

SD <sub>elevation</sub> – Ranking Scores						
Landslide ID	3×3	5×5	7×7	9×9	11×11	Total
12	1	1	1	1	1	5
13	1	1	1	1	1	5
14	3	3	3	3	3	15
15	2	2	2	2	2	10
16	3	3	3	3	3	15

After the score has been calculated for each landslide using the three measures of surface texture (SD<sub>slope</sub>, SD<sub>profile</sub>, and SD<sub>elevation</sub>), the scores are summed to provide a total score. This total score is representative of the relative surface texture, or roughness, across the project site. Table 7 lists the relative roughness score for each landslide identified at the Little Smoky project site.

**Table 7. Relative landslide surface texture total ranking score.**

Landslide ID	SD <sub>elevation</sub>	SD <sub>profile</sub>	SD <sub>slope</sub>	Relative Roughness Score
1	5	6	5	16
2	5	5	5	15
3	10	10	12	32
6	15	15	15	45
7	10	10	10	30
8	10	10	10	30
9	15	15	15	45
10	10	10	10	30
11	5	5	9	19
12	5	5	5	15
13	5	5	5	15
14	15	15	15	45
15	10	12	15	37
16	15	15	15	45

The relative roughness score is used to rank the landslides from least rough to most rough. We have grouped the results, scores ranging from 15 to 45, into three classes. The least rough class encompasses relative roughness scores from 15 to 25, the middle or medium relative roughness class has scores from 26 to 35, and the most rough class includes landslides with relative roughness scores of 36 to 45. Each landslide was grouped into one of three classes so that the results could be compared to the three classes of measured displacement shown in Figure 5.

The results of the relative surface texture analysis are shown in Figure 10. The landslides are coloured based on their relative roughness score and show the distribution of surface texture or roughness across the site.

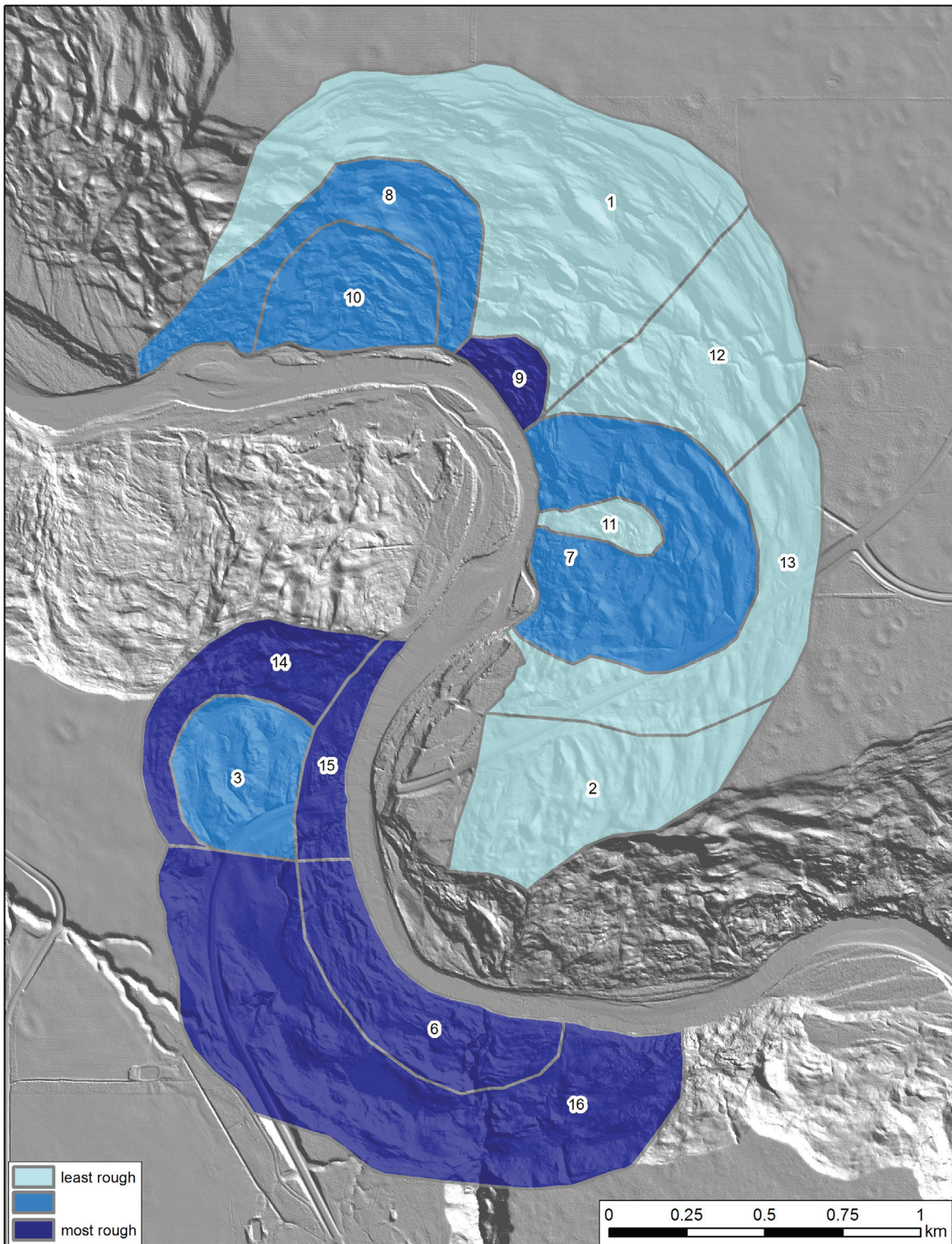


Figure 10. Landslide map showing relative levels of surface roughness. Numbers represent landslide ID.

## 5 Discussion and Conclusion

The relative roughness scoring system correlates well to the three classes of measured displacement for the majority of landslides at the Little Smoky River Highway 49 river crossing. Landslides 2, 7, 13, and 15 all show roughness classifications that can be correlated to the three ranges of measured horizontal displacement shown in Figure 5. More specifically, the displacement range of 5 to 40 mm can be considered equivalent to the least rough classification, the displacement range of 40 to 90 mm to the medium rough classification, and the range above 90 mm to the most rough classification. These results are promising and show that the method can be useful to empirically predict the activity classification for those landslides that do not have displacement information. The relative classifications of landslides 1, 9, 8, 10, 11, and 12 are considered analogous to three classes of expected displacement with good confidence. It is perhaps difficult to state that the predicted displacement would exactly match the three ranges of displacement measured at the project site and shown in Figure 5, but there is good confidence that the relative roughness classifications are an indicator of relative landslide activity.

However, the method described in this report did not provide the same correlations for landslides 3, 6, and 16. These landslides returned a roughness signature that predicted a movement range higher than the measured displacement. These landslides are located on the west side of the Little Smoky River. Although these landslides have a similar translational style of movement, the failure surface is shallower than on the east side, the average slope angles are slightly higher, and the morphology of the slides is dominated by large backscarps at the head of the landslide zones. In addition, grading and drainage activities on the eastern approach to the bridge have also contributed to a different morphology than on the east side, which may be contributing to the misleading results from the relative roughness analysis. It is also worth mentioning that the measured displacements on the west side of the river tend to be clustered close to the roadway and may not accurately reflect the movement characteristics across the landslide areas, most notably to the south where instrumentation coverage is non-existent. Regardless, there is a lower confidence that the results of the relative roughness analysis correlate to the relative activity on the western slopes. These results highlight the fact that although spatial analysis methods can provide useful metrics for considering the relative activity state of the landslides at the Little Smoky River Highway 49 crossing site, a good understanding of subsurface geological setting is of utmost importance, and expert judgement must be an integral part of the spatial analysis process.

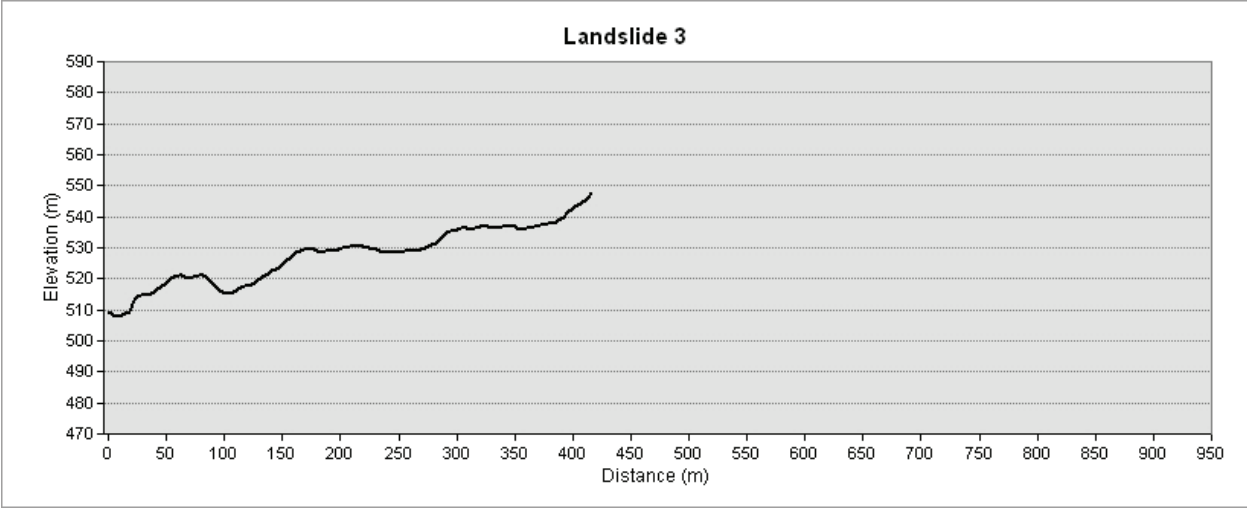
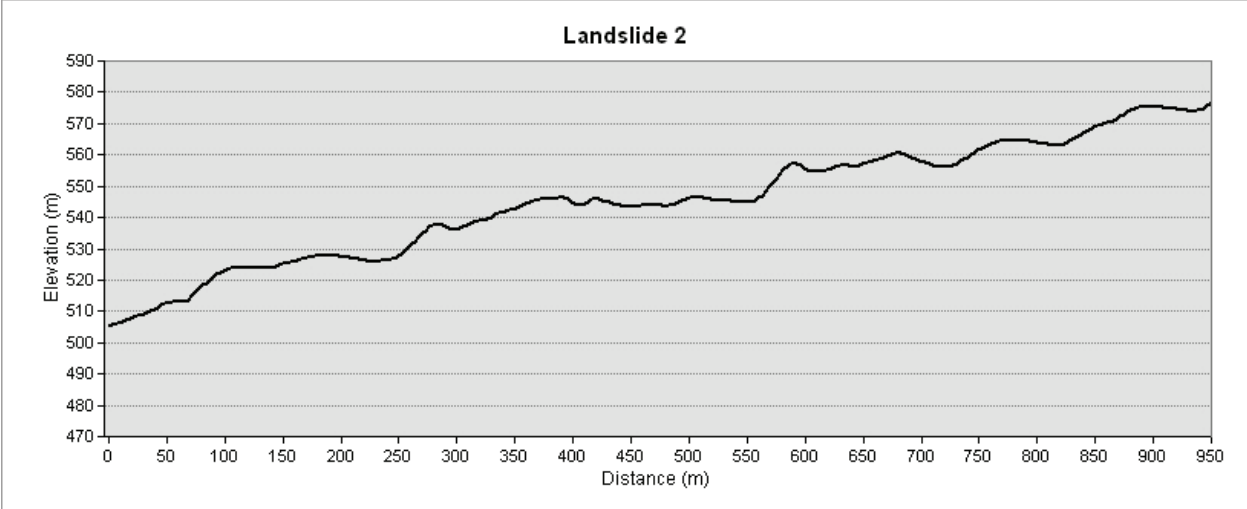
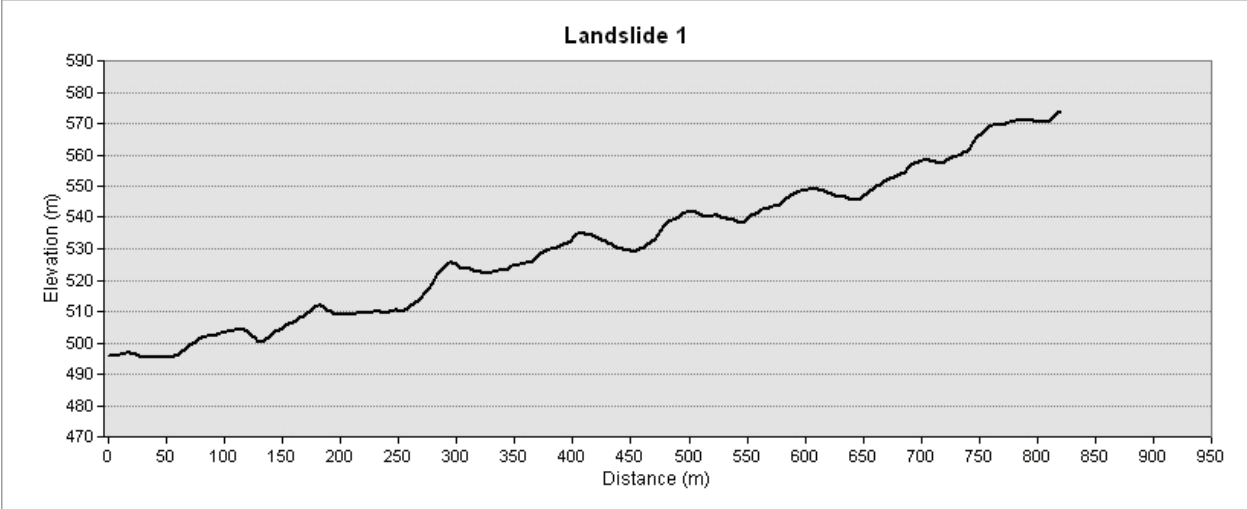
## 6 References

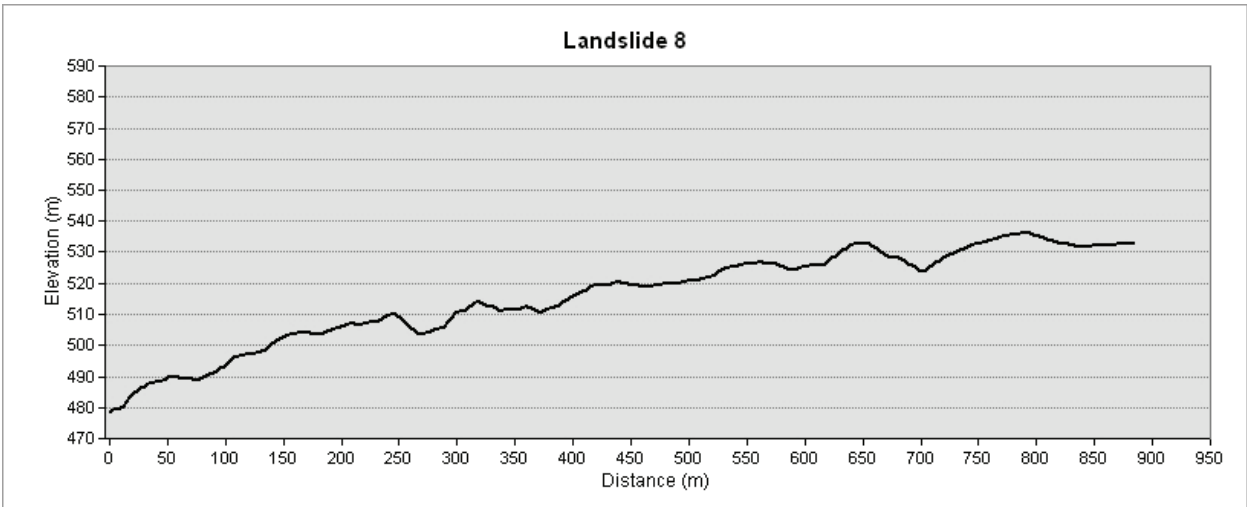
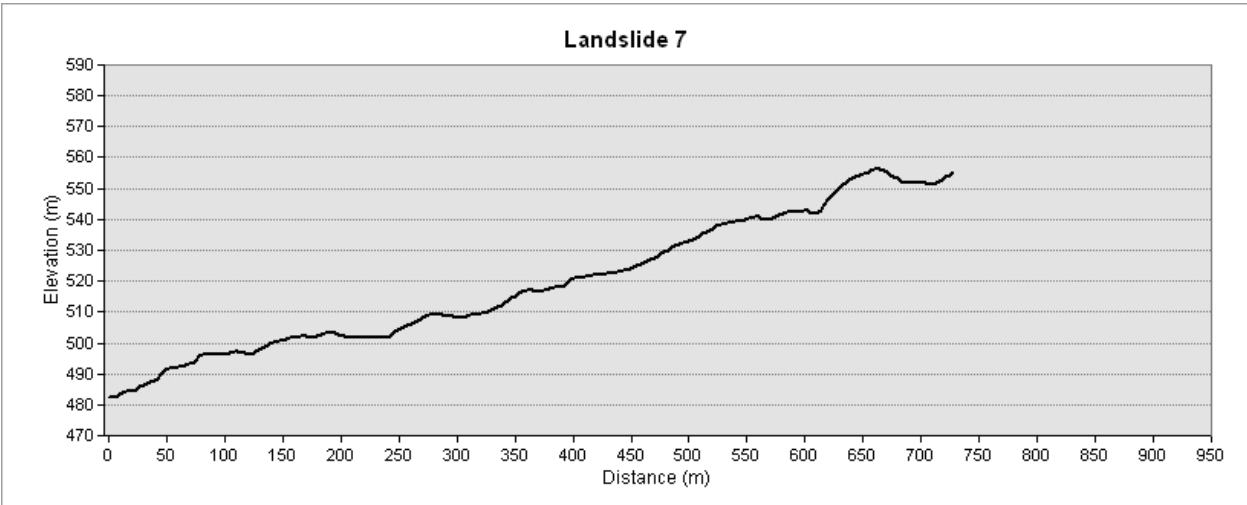
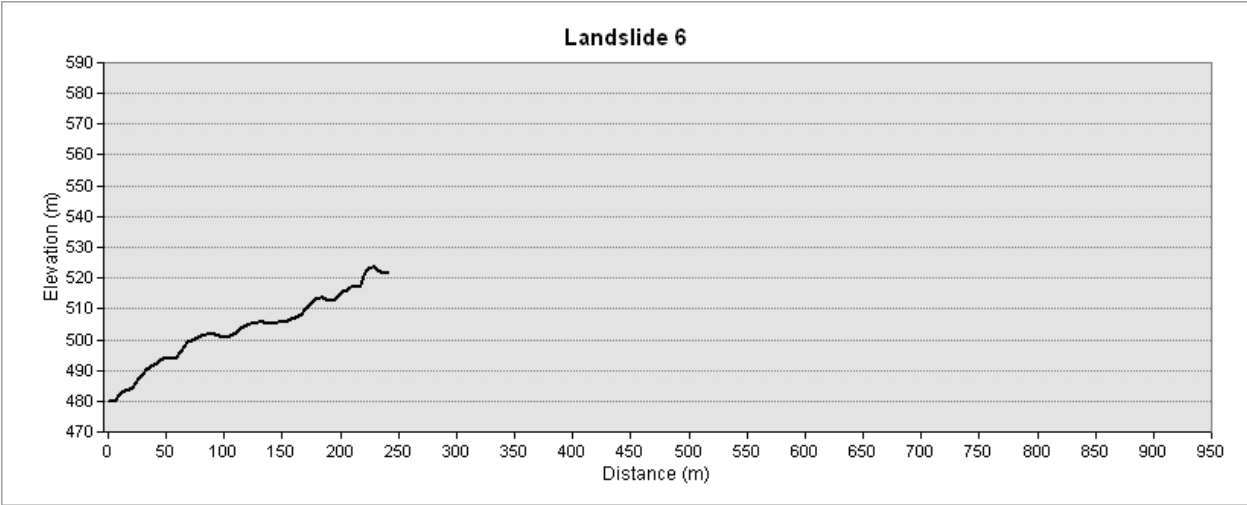
- Cruden, D.M. and Varnes, D.J. (1996): Landslides types and processes; in Landslides: investigation and mitigation, A.K. Turner and R.L. Schuster (ed.), Transportation Research Board, Special Report 247, National Academy Press, Washington, D.C., p. 36–75.
- Froese, C.R. (2004): Little Smoky River InSAR Assessment of Slope Movement; AMEC Earth & Environmental, File No. EG09024, prepared for Alberta Infrastructure and Transportation.
- Froese, C.R., Poncos, V., Skirrow, R., Mansour, M. and Martin, D. (2008): Characterizing complex deep seated landslide deformation using corner reflector InSAR (CR-InSAR): Little Smoky Landslide, Alberta; in Proceedings of the 4th Canadian Conference on Geohazards, Quebec City, Quebec, p. 287-293.
- Grohmann, C.H., Smith, M.J., and Riccomini, C. (2011). Multiscale analysis of topographic surface roughness in the Midland Valley, Scotland. IEEE Transactions on Geoscience and Remote Sensing, Vol. 49, No. 4.
- J.D. Mollard & Associates Limited, May 1997, Office Airphoto and Map Study of the Little Smoky River Valley Upstream and Downstream From Highway 43 Bridge, prepared for Alberta Transportation.
- Morgan, A.J., Chao, D.K. and Froese, C.R. (2013): LiDAR-based landslide classification and inventory, Peace River, Alberta (NTS 84C); Energy Resources Conservation Board, ERCB/AGS Open File Report 2013-01, 22 p., URL <[http://www.ags.gov.ab.ca/publications/abstracts/OFR\\_2013\\_01.html](http://www.ags.gov.ab.ca/publications/abstracts/OFR_2013_01.html)> [May 2013].
- Skirrow, R., Proudfoot, D., Froese, C.R. and Thomson, S. (2005): Update on the Little Smoky landslide. 58th Canadian Geotechnical Conference, Saskatoon, SK, URL <[http://www.transportation.alberta.ca/Content/docType253/Production/GS509\\_secured.pdf](http://www.transportation.alberta.ca/Content/docType253/Production/GS509_secured.pdf)> [May 2013].
- Thomson, S. and Hayley, D.W. (1975): The Little Smoky landslide; Canadian Geotechnical Journal, v.12, p. 379–392.

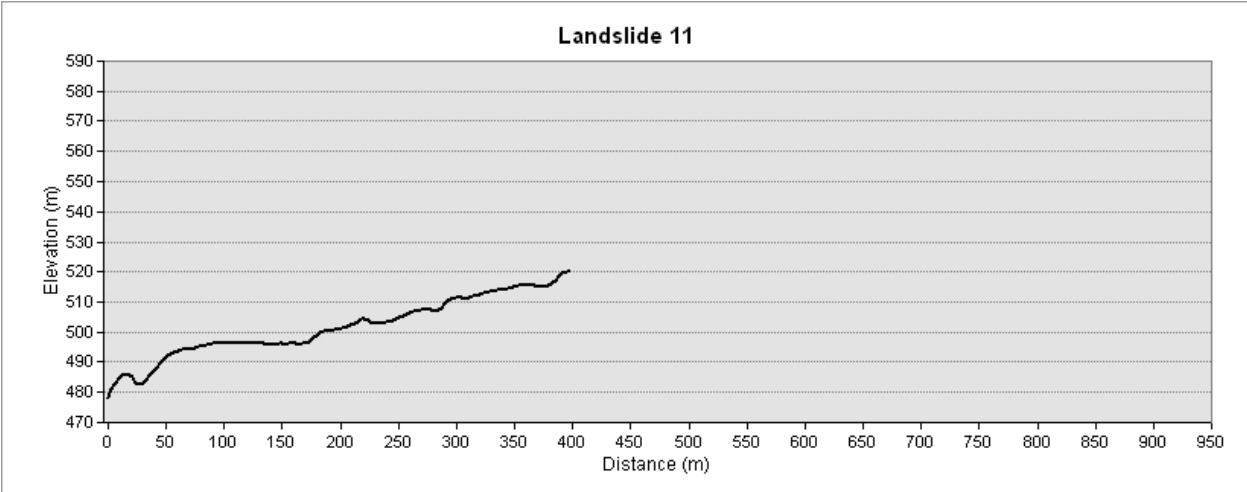
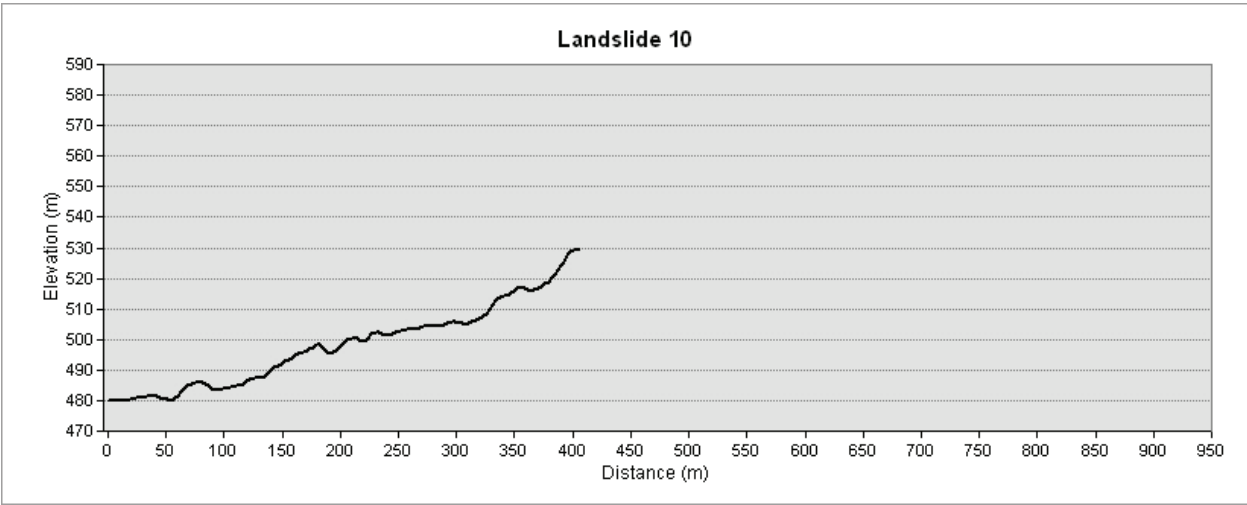
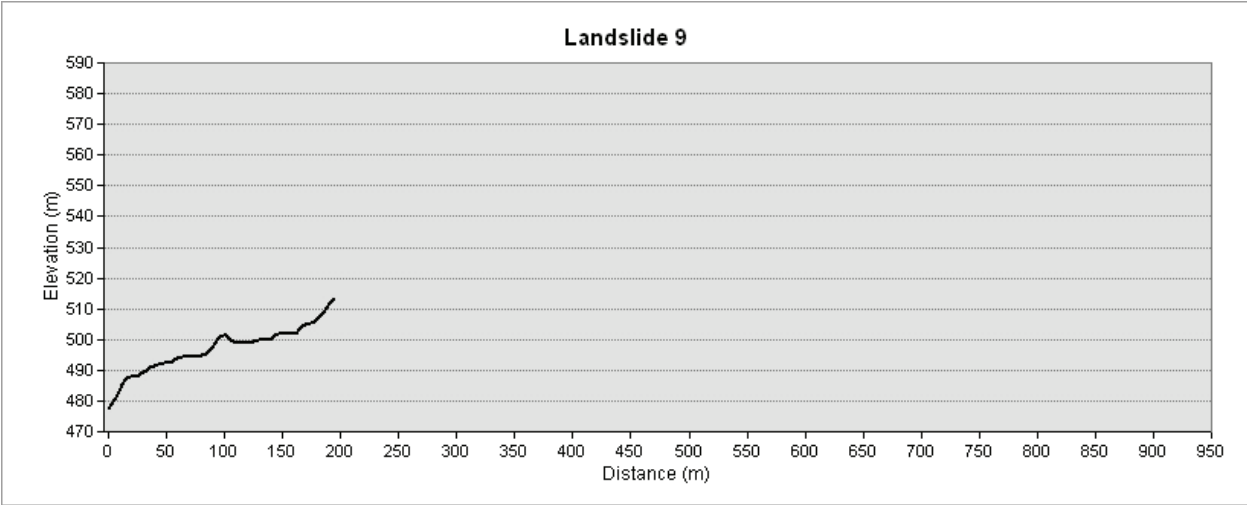
## Appendix 1 – Landslide Key Map and Elevation Profiles

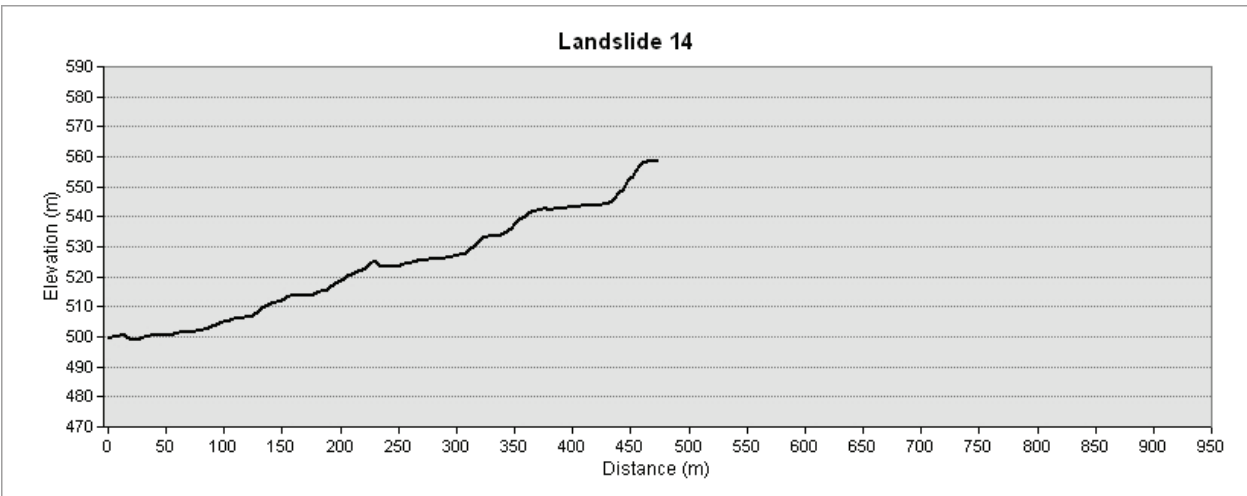
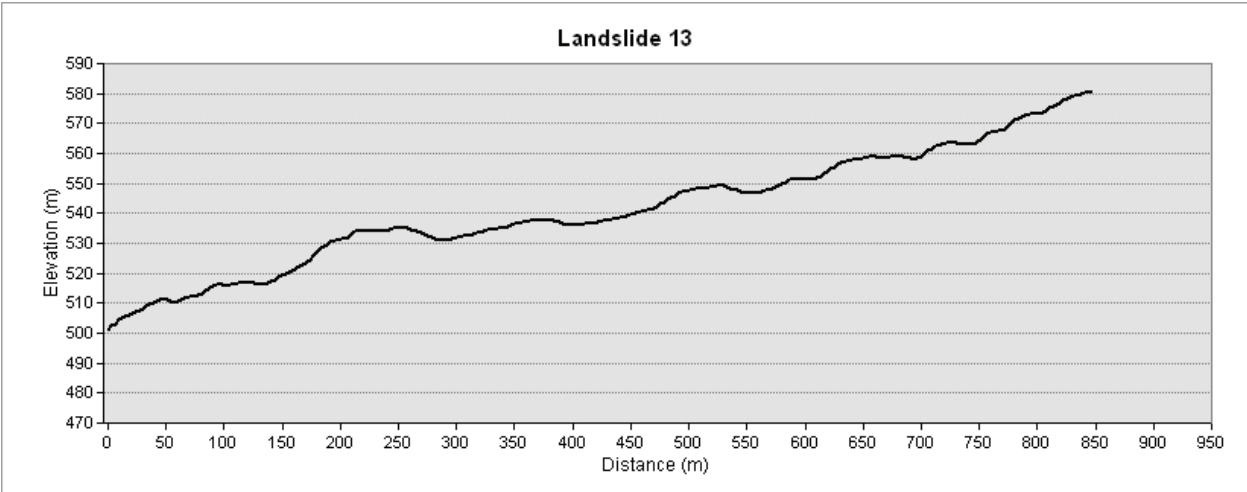
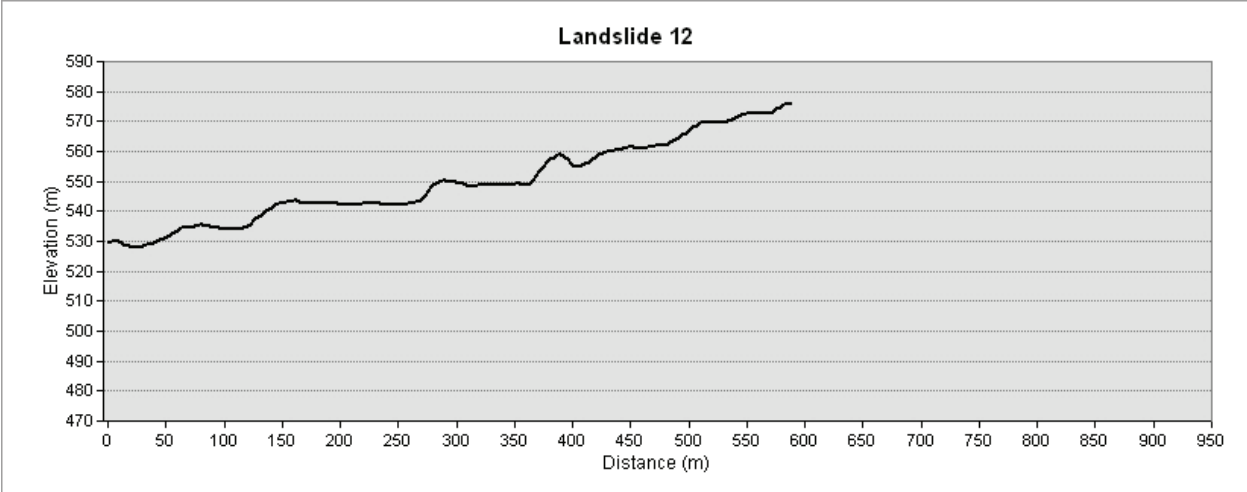


Figure 11. Key map showing landslide boundaries, identification numbers, and profile lines.









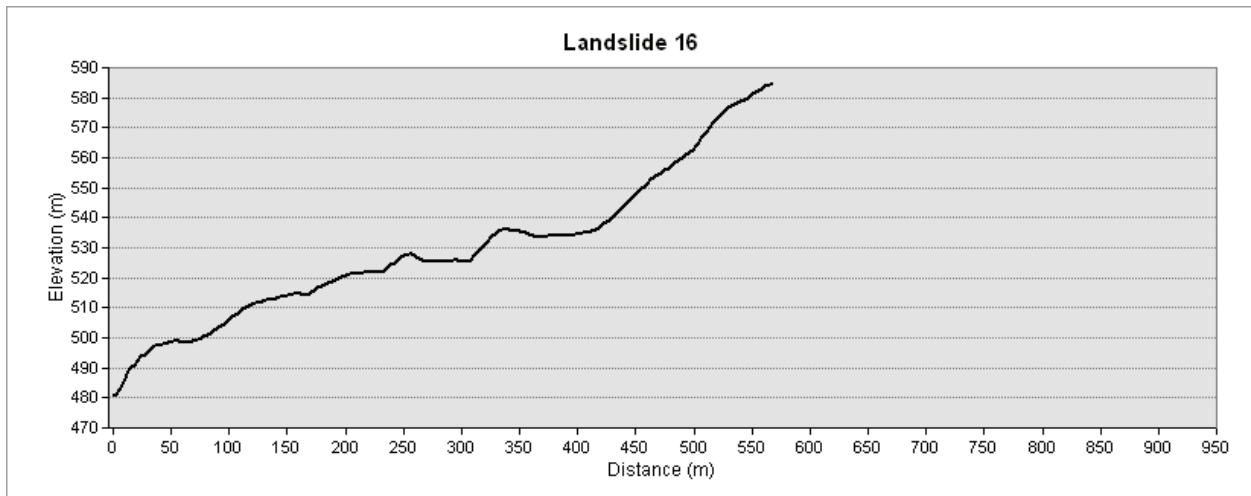
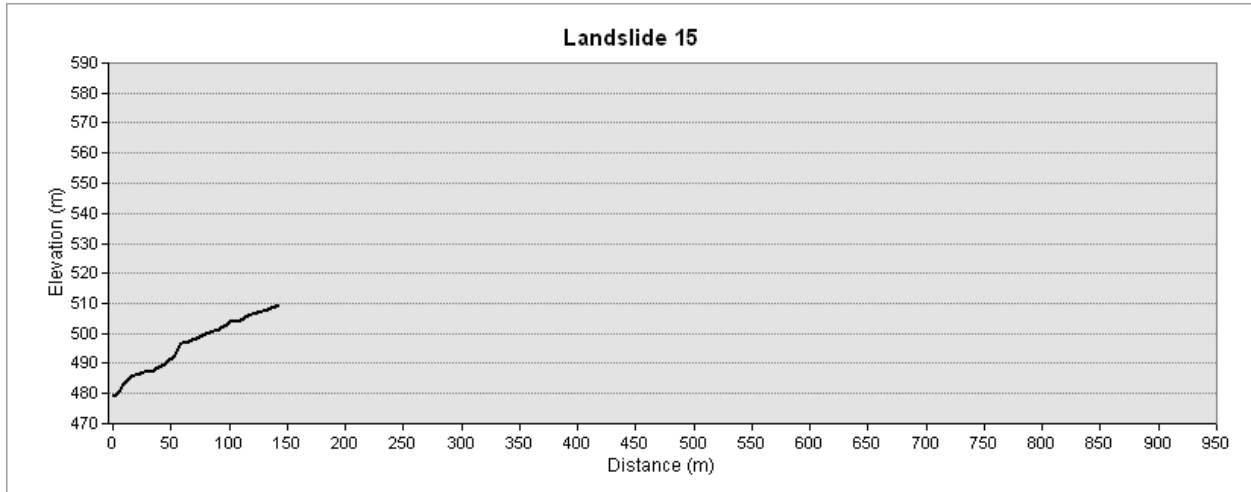


Figure 12. Elevation profile lines for each landslide as shown in plan on Figure 11.

## Appendix 2 – Grid Statistics

$SD_{profile}$

**Table 8. Minimum and maximum values obtained from the combined  $SD_{profile}$  grid. These values are used to normalize the grid and create the combined normalized  $SD_{profile}$  grid.**

$SD_{profile}$	3×3	5×5	7×7	9×9	11×11
Min	0.02034505	0.04465911	0.08794846	0.14177625	0.17015819
Max	51.5034447	42.778038	35.56987	34.4774628	32.1368675

Diff = 51.4830996

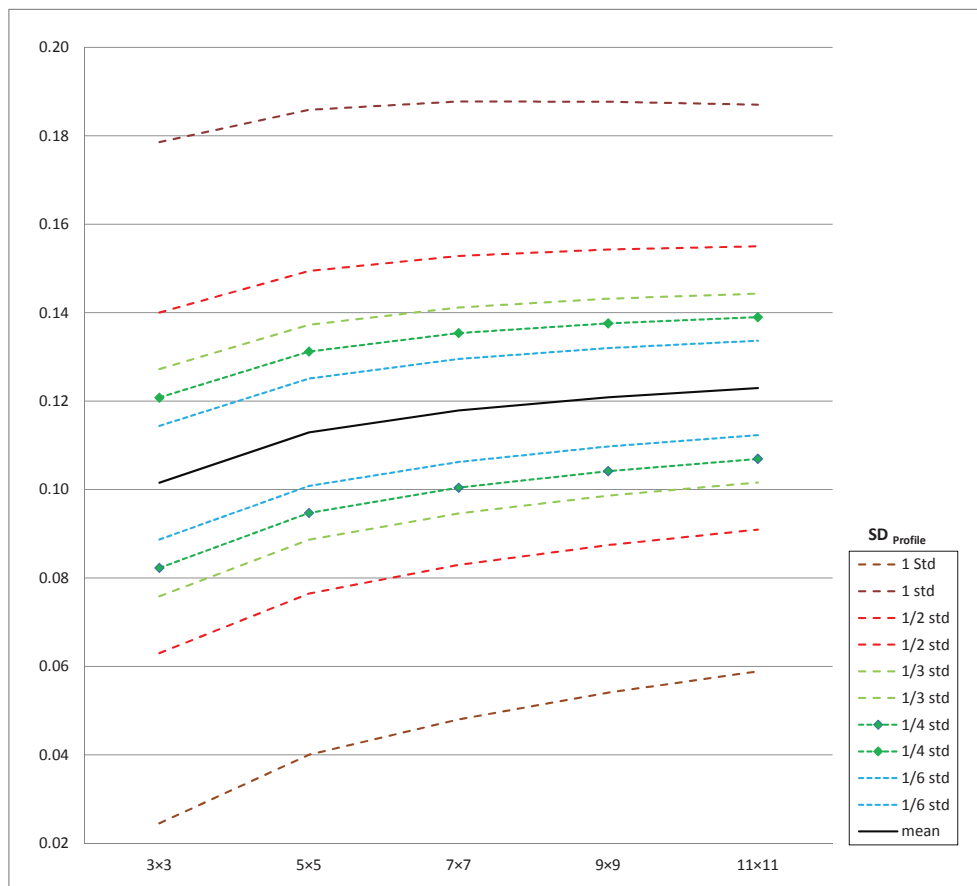


**Figure 13. Mean and standard deviation values calculated from the combined normalized  $SD_{profile}$  grid, which considers all the surface area across all the defined landslide polygons.**

**Table 9. Mean, standard deviation, maximum, and minimum values calculated from the combined normalized  $SD_{profile}$  grid.**

$SD_{profile}$	3×3	5×5	7×7	9×9	11×11
Mean	0.10153	0.07700	0.11294	0.07293	0.11788
Std Dev	0.07700	0.11294	0.07293	0.11788	0.06987
Max	0.11436	0.12510	0.12953	0.13199	0.13363
Min	0.08870	0.10079	0.10624	0.10973	0.11227

**Table 10. Mean values calculated for each landslide area using the clipped normalized  $SD_{profile}$  grid.**

	3×3	5×5	7×7	9×9	11×11
<b>Id</b>	<b>Mean</b>	<b>Mean</b>	<b>Mean</b>	<b>Mean</b>	<b>Mean</b>
1	0.08643	0.09668	0.10130	0.10416	0.10627
2	0.07518	0.08337	0.08706	0.08923	0.09079
3	0.11183	0.12396	0.12914	0.13234	0.13462
6	0.13813	0.15369	0.16004	0.16352	0.16573
8	0.09663	0.10722	0.11176	0.11445	0.11640
9	0.10581	0.11809	0.12337	0.12639	0.12844
10	0.13941	0.15613	0.16288	0.16636	0.16853
11	0.10857	0.12110	0.12650	0.12945	0.13144
12	0.09260	0.10269	0.10720	0.10981	0.11157
13	0.08323	0.09271	0.09710	0.09978	0.10167
15	0.07620	0.08456	0.08808	0.09021	0.09162
16	0.12367	0.13693	0.14218	0.14515	0.14704
7	0.11767	0.13118	0.13688	0.14019	0.14234
14	0.12392	0.13751	0.14341	0.14723	0.15000

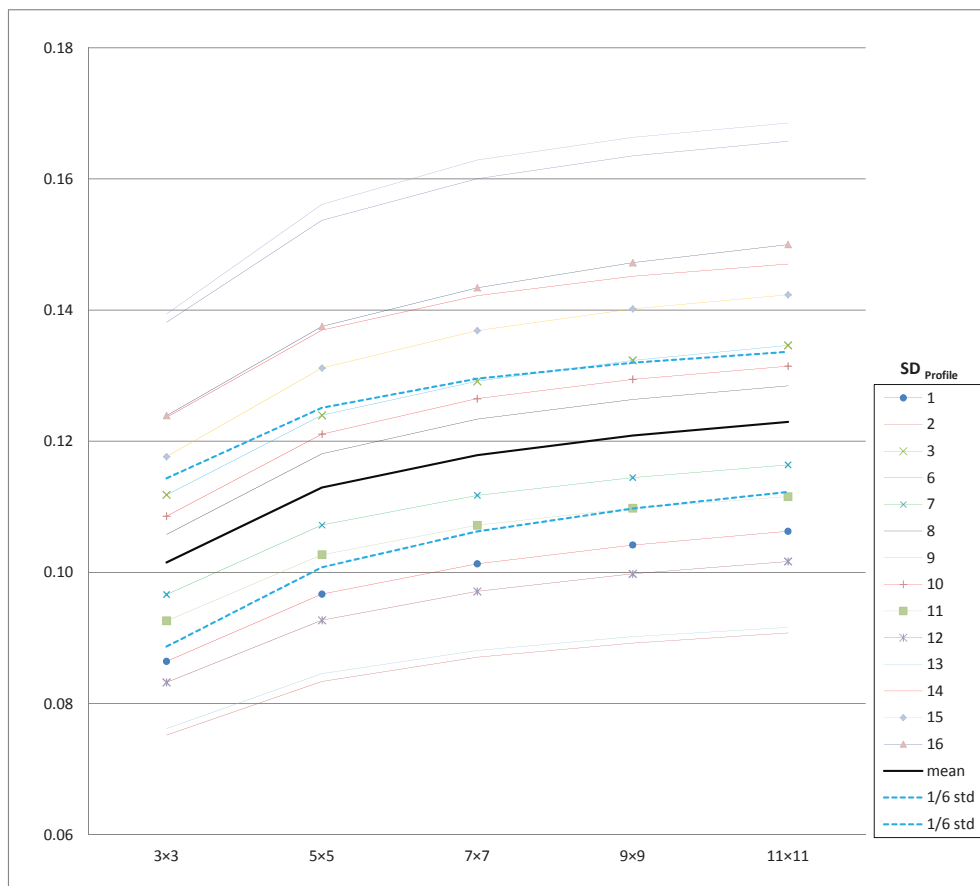


**Figure 14. Mean values calculated for  $SD_{profile}$  for each landslide ID (coloured lines) compared to the mean for the combined normalized  $SD_{profile}$  grid (black line), with 1/6th standard deviation thresholds shown (SD).**

**SD<sub>elevation</sub>**

**Table 11. Minimum and maximum values obtained from the combined SD<sub>elevation</sub> grid. These values are used to normalize the grid and create the combined normalized SD<sub>elevation</sub> grid.**

SD <sub>elevation</sub>	3×3	5×5	7×7	9×9	11×11
Min	0.0	0.00634711	0.00867692	0.01135516	0.01452292
Max	5.5777216	6.07445955	7.22429371	8.33823586	9.03813171

Diff = 9.03813

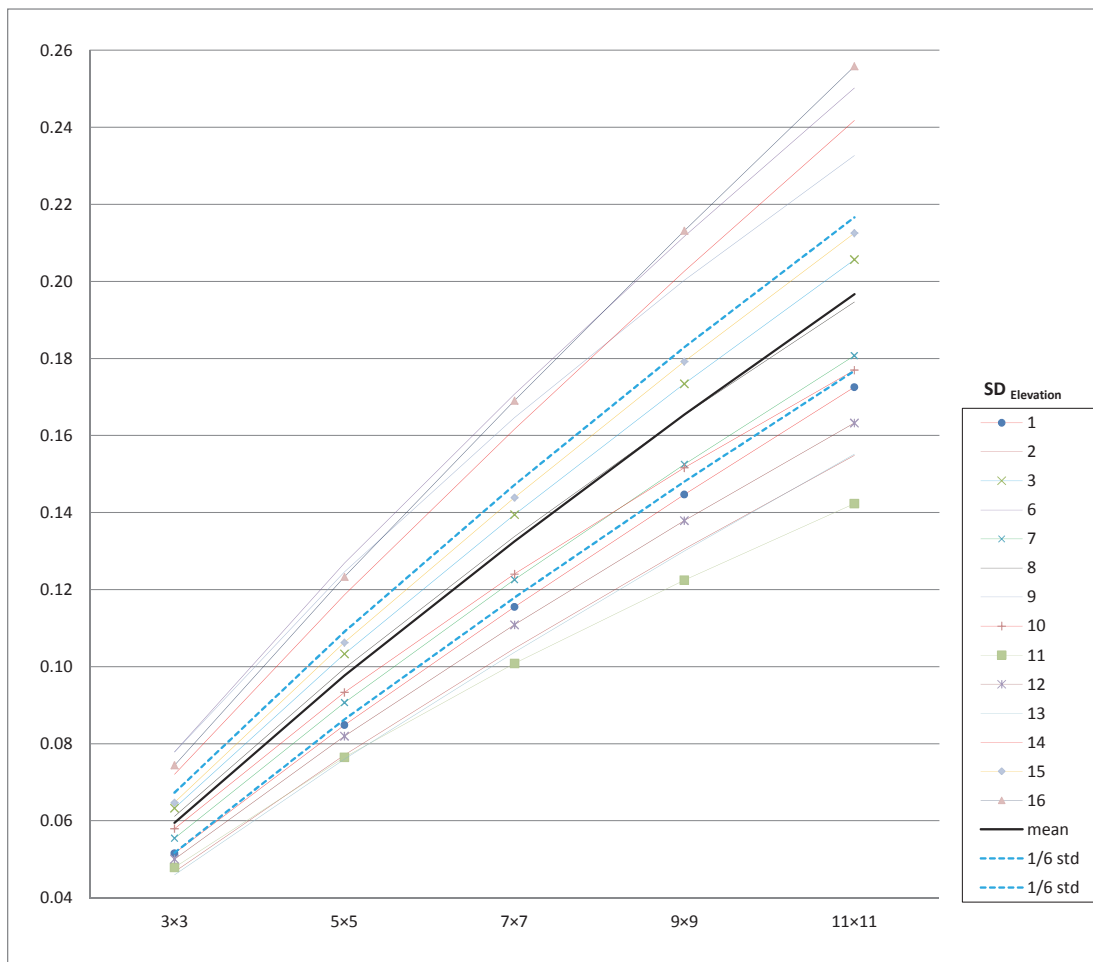


**Figure 15. Mean and standard deviation values calculated from the combined normalized SD<sub>elevation</sub> grid, which considers all the surface area across all the defined landslide polygons.**

**Table 12. Mean, standard deviation, maximum, and minimum values calculated from the combined normalized SD<sub>elevation</sub> grid.**

SD <sub>elevation</sub>	3×3	5×5	7×7	9×9	11×11
Mean	0.05948	0.04672	0.09766	0.06826	0.13250
Std Dev	0.04672	0.09766	0.06826	0.13250	0.08768
Max	0.06726	0.10903	0.14711	0.18285	0.21660
Min	0.05169	0.08628	0.11789	0.14800	0.17676

**Table 13. Mean values calculated for each landslide area using the clipped normalized  $SD_{\text{elevation}}$  grid.**

	3×3	5×5	7×7	9×9	11×11
<b>Id</b>	<b>Mean</b>	<b>Mean</b>	<b>Mean</b>	<b>Mean</b>	<b>Mean</b>
1	0.05155	0.08483	0.11548	0.14468	0.17257
2	0.04675	0.07707	0.10469	0.13056	0.15484
3	0.06326	0.10330	0.13945	0.17343	0.20567
6	0.07785	0.12685	0.17074	0.21168	0.25022
8	0.05545	0.09068	0.12258	0.15251	0.18076
9	0.06116	0.09958	0.13377	0.16532	0.19466
10	0.07778	0.12461	0.16461	0.20031	0.23267
11	0.05794	0.09333	0.12402	0.15166	0.17698
12	0.04787	0.07648	0.10082	0.12245	0.14233
13	0.05005	0.08195	0.11088	0.13792	0.16328
15	0.04596	0.07598	0.10368	0.13001	0.15516
16	0.07206	0.11864	0.16163	0.20261	0.24178
7	0.06473	0.10628	0.14389	0.17919	0.21252
14	0.07442	0.12332	0.16902	0.21317	0.25584

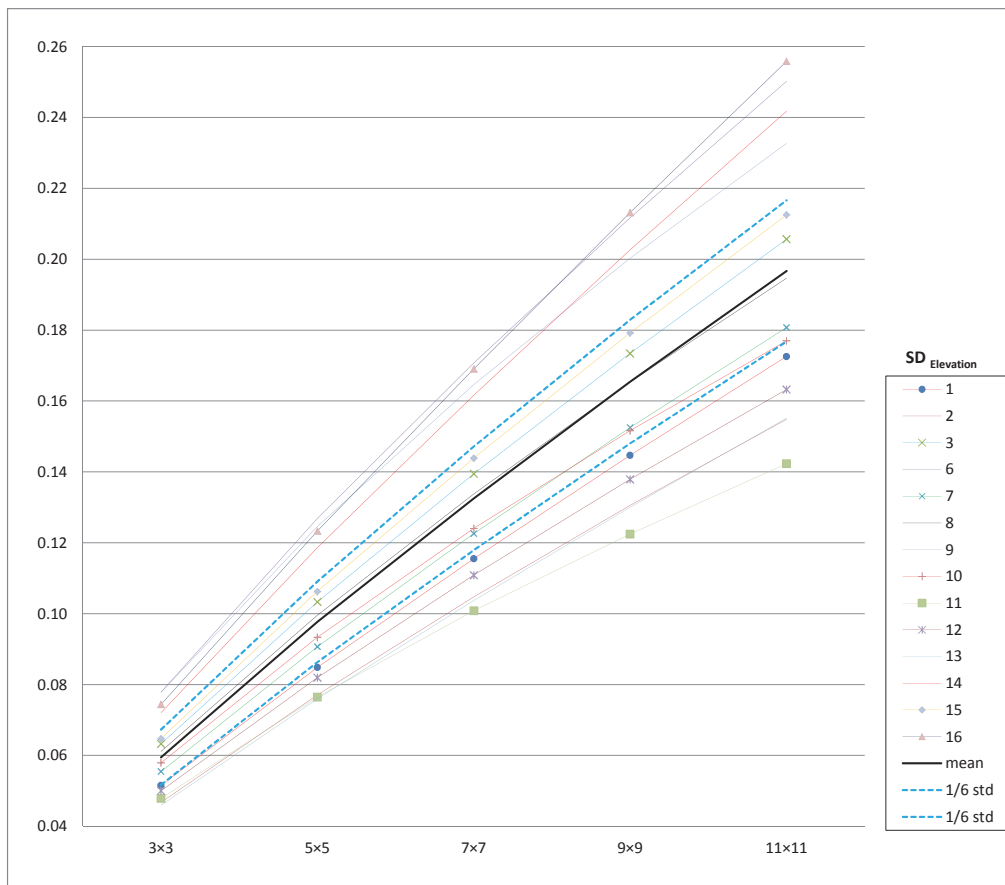


**Figure 16.  $SD_{\text{elevation}}$  mean values calculated for  $SD_{\text{elevation}}$  for each landslide ID (coloured lines) compared to the mean for the combined normalized  $SD_{\text{elevation}}$  grid (black line), with 1/6th standard deviation thresholds shown (SD).**